is promoted by electronic excitation. Therefore, the reaction from **3** to **4** seemed to be accelerated by laser illumination as well as by thermal excitation.

In conclusion, resonance Raman spectra for autoxidation intermediates of ferrous porphyrin were obtained and they are consistent with eqs 1–4 deduced from NMR spectroscopy.[14c] Some additional new information obtained here demonstrated the presence of the Fe^{II}—O_2 complex at −100 °C and the Fe^{IV}=O complex at −70 °C, although they are photolabile, and suggested that reduction of the Fe^{IV}=O porphyrin proceeds via hydrogen abstraction from solvent (toluene).

Acknowledgment. This work was partly supported by Grant-in-Aids for Scientific Research in Priority Area to T.K. (63635005) and to Y.T. (62607516) from the Ministry of Education, Science, and Culture.

(Tetrakis(2-pyridylmethyl)ethylenediamine)iron(II) Perchlorate, the First Rapidly Interconverting Ferrous Spin-Crossover Complex

Hsiu-Rong Chang,[1] James K. McCusker,[1,2] Hans Toftlund,*[,3] Scott R. Wilson,[1] Alfred X. Trautwein,[4] Heiner Winkler,[4] and David N. Hendrickson*[,2]

Contribution from the School of Chemical Sciences, University of Illinois, Urbana, Illinois 61801, Department of Chemistry, D-0506, University of California at San Diego, La Jolla, California 92093-0506, Department of Chemistry, University of Odense, DK-5230 Odense M, Denmark, and Department of Physics, Medizinische Universitat, 2400 Lübeck 1, West Germany.
Received November 20, 1989. Revised Manuscript Received March 20, 1990

Abstract: The preparation and characterization of the first Fe^{II} spin-crossover complex that interconverts between high- and low-spin states at a rate faster than the ^{57}Fe Mössbauer time scale is reported. $[Fe(tpen)](ClO_4)_2 \cdot {}^2/_3H_2O$ crystallizes in the monoclinic space group $C2/c$, which at 298 K has a unit cell of a = 40.87 (2) Å, b = 9.497 (4) Å, c = 23.946 (9) Å, and β = 108.42 (4)° with Z = 12 and at 358 K the unit cell is characterized by a = 41.00 (2) Å, b = 9.517 (5) Å, c = 24.21 (1) Å, and β = 109.46 (4)° with Z = 12. The hexadentate ligand tpen is tetrakis(2-pyridylmethyl)ethylenediamine. The refinements were carried out with 3110 (2.58σ) and 2221 (2.58σ) observed reflections at 298 and 358 K, respectively, to give R = 0.073 and R_w = 0.076 at 298 K and R = 0.082 and R_w = 0.082 at 358 K. At both temperatures there are two crystallographically different $[Fe(tpen)]^{2+}$ cations. One of these two cation sites has a greater high-spin content, as evidenced by Fe–ligand atom bond lengths and trigonal distortions which are greater than those found at the other cation site. The Fe–N bond lengths and trigonal distortion increase for both cations as the temperature is increased from 298 to 358 K. Solid-state magnetic susceptibility data show that the critical temperature, T_c, where there are equal amounts of high- and low-spin complexes, is T_c = 365 K. Faraday balance data for this same perchlorate salt in DMF solution give T_c = 363 K. The similarity of these solid- and solution-state T_c values and the susceptibility data taken for the pure solid and solid solutions in the isostructural Zn^{2+} complex definitively show that the spin-crossover cations in $[Fe(tpen)](ClO_4)_2 \cdot {}^2/_3H_2O$ experience no appreciable intermolecular interactions. Each cation acts independently in a high-/low-spin equilibrium. The ^{57}Fe Mössbauer spectrum exhibits only one quadrupole-split doublet for each cation up to the highest temperature (350 K) investigated. Thus, this is the first Fe^{II} spin-crossover complex that interconverts in the solid state between high- and low-spin states at a rate that is faster than the Mössbauer time scale. A careful analysis of the changes in the structure of the $[Fe(tpen)]^{2+}$ cation as a function of temperature together with angular overlap calculations suggest that it is the increase in Fe–N bond lengths together with an increase in the trigonal distortion that leads to the fast rate of spin-state interconversion in $[Fe(tpen)]^{2+}$. The steric constraints introduced by the hexadentate ligand lead to a relatively large trigonal distortion lowering the energy of triplet excited states ($^3T_1$ and/or $^3T_2$). This then leads to greater spin–orbit interaction of the ^1A low-spin state with components of the $^5T_2$ high-spin state, and a greater rate of interconversion results. Additional evidence supporting the presence of fluxional distortions of $[Fe(tpen)]^{2+}$ along a trigonal twisting coordinate is presented in the form of variable-temperature ^1H NMR data. In solution $[Fe(tpen)]^{2+}$ exhibits a very fast rate (>600 s^{-1}) of enantiomerization. Finally, the preparation and properties (T_c > 400 K) of $[Fe(tpen)](ClO_4)_2$ are given. This non-hydrated complex crystallizes in the monoclinic space group $P2_1/c$, which at 298 K has a unit cell characterized by a = 17.865 (3) Å, b = 9.878 (1) Å, c = 17.213 (4) Å, and β = 110.01 (2)° with Z = 4. This structure was refined with 3031 (2.58σ) observed reflections to give R = 0.049 and R_w = 0.053. The trigonal twist found for the cation is in keeping with magnetic susceptibility data indicating that this nonhyrated complex is totally low spin at 298 K.

Introduction

In addition to oxygenation and carbonylation of myoglobin and hemoglobin, electron-transfer reactions of heme proteins are often associated with a change in the spin-state of an iron ion from high spin to low spin and vice versa.[5] For example, there has been considerable interest in the coupling of spin, substrate, and redox equilibria in cytochrome P450.[6] It has been shown that the

(1) University of Illinois.
(2) University of California at San Diego.
(3) University of Odense.
(4) Medizinsche Universitat.

(5) (a) Dose, E. V.; Tweedle, M. F.; Wilson, L. J.; Sutin, N. *J. Am. Chem. Soc.* **1977**, *99*, 3886. (b) Dyson, H. J.; Beattie, J. K. *J. Biol. Chem.* **1982**, *257*, 2267. (c) George, P.; Beetlestone, J.; Griffith, J. S. *Rev. Mod. Phys.* **1964**, *36*, 441. (d) Ogunmola, G. B.; Kauzmann, W.; Zipp, A. *Proc. Natl. Acad. Sci. U.S.A.* **1976**, *73*, 4271. (e) Fisher, M. T.; Sligar, S. G. *Biochemistry* **1987**, *26*, 4797.
(6) (a) Raag, R.; Poulus, T. L. *Biochemistry* **1989**, *28(2)*, 917. (b) Moura, I.; Liu, M. Y.; Costa, C.; Liu, M. C.; Pai, G.; Xavier, A. V.; LeGall, J.; Payne, W. J.; Moura, J. J. G. *Eur. J. Biochem.* **1988**, *177(3)*, 673.

0002-7863/90/1512-6814$02.50/0

spin-state equilibrium serves to modulate both the substrate binding as well as the redox potential of this cytochrome. In addition to this biological relevance, fundamental interest in spin-state interconversion rates has led to considerable research on spin-crossover complexes.[7]

Much of the work in this area has concentrated on spin-state interconversions in the solid state. The interrelationships between the factors controlling intramolecular dynamics and intermolecular interactions in the solid state have not yet been delineated completely, although some advances have been made resulting from theoretical studies.[8] Ever since the benchmark heat-capacity study of Sorai and Seki,[8c] it has been clear that spin-crossover transformations that occur abruptly over a small temperature range do so cooperatively as first-order phase transitions. At the other extreme are systems that exhibit a "spin-equilibrium" where there are no intermolecular interactions and there is a Boltzmann population of high- and low-spin complexes. The phase transitions for each spin-crossover complex can be characterized by determining into which universal class[9] each phase transition belongs.

Recently Gütlich et al.[10] reported the interesting phenomenon of "light-induced excited-spin-state trapping" (LIESST). It was found that upon exposure to light (xenon lamp) for a period of several minutes, crystalline samples of certain Fe^{II} spin-crossover complexes maintained at temperatures near to liquid-helium temperatures could be completely converted from low spin to high spin. What is so remarkable is that once these Fe^{II} complexes are converted to the high-spin state they will remain in the high-spin state for hours or even days if the sample is maintained at low temperature. Herber and Casson[11] have shown that FTIR spectra could also be used to monitor the LIESST phenomenon. Very recent work[12] has suggested that the slow kinetics that are being monitored in these observations are attributable to individual complexes tunneling between high- and low-spin states, not to the kinetics of domain walls found in cooperative phase transitions.

However, there has been surprisingly little work aimed at determining the factors that control the rate and mechanism of spin-state interconversion in an isolated spin-crossover complex. Laser Raman temperature-jump[13] and ultrasonic relaxation measurements[14] have been carried out for spin-crossover complexes in solution over a limited temperature range near room temperature. Beattie[7g] has recently published a review that concentrates on the dynamics of spin equilibria in solution. Very recently, the laser flash-photolysis technique was used to study the relaxation kinetics of a ferrous spin-crossover complex doped at low concentration into a polymer film.[15] From room temperature down to approximately 120 K, rate data were found to exhibit Arrhenius-type behavior. In the range of 120 to 4.2 K, however, the relaxation rate became independent of temperature. This was interpreted as direct evidence of quantum mechanical tunneling as the mechanism of interconversion.[15a] A fit of the experimental data to theoretical models indicated that thermally activated tunneling was also the predominant mechanism in the 120–300 K range. Conti et al.[15b] have recently shown that spin-state interconversion relaxation rates can also be concentration dependent. On the basis of conductivity measurements, they suggested that ion-aggregation in solution plays a role in determining the characteristics of spin-state equilibria even in a dilute environment.

In this paper we report the detailed characterization of the first simple Fe^{II} spin-crossover complex to interconvert in the solid state at a rate that is faster than the time scale of the Mössbauer experiment. It will be shown that the dynamics of this complex are little affected by intermolecular interactions in the solid state. This system thus represents a true spin equilibrium system even as a solid. The intramolecular factors that may lead to the fast rate of spin-state interconversion in this complex will be discussed. It is shown that a twist distortion of the Fe^{II} complex is linked to the fast rate of spin-state interconversion. Support for this is found in a relatively fast rate of enantiomerization noted for the same Fe^{II} complex in solution. The idea of linking ligand psuedorotation and spin-state conversion has been discussed for several years.[16]

Experimental Section

Compound Preparations. All reagents were commercially available and used without further purification. All synthetic procedures involving Fe^{II} complexes were performed under an inert Ar atmosphere, using standard Schlenk techniques.

***N,N,N',N'*-Tetrakis(2-pyridylmethyl)-1,2-ethylenediamine (tpen).** This compound was prepared by a modification of a previously reported method.[17] 2-Picolyl chloride hydrochloride (6.56 g, 60.0 mmol; Aldrich) in 5 mL of water was neutralized by slow addition of 7.4 mL of a 5.4 M NaOH solution. To this solution 0.67 mL (10 mmol) of ethylenediamine was added dropwise. The reaction mixture was allowed to stir at room temperature for 4 days. During this time, the pH of the mixture was maintained between 7 and 9 by periodic dropwise addition of a 4 M solution of NaOH. A white precipitate, formed initially after 2 or 3 days, was then filtered, washed with a small amount of water (ca. 30 mL), and dried in vacuo for 24 h. Anal. Calcd for $C_{26}H_{28}N_6$: C, 73.58; H, 6.60; N, 19.81. Found: C, 73.54; H, 5.86; N, 19.68.

$FeCl_2 \cdot 2H_2O$. Commercially available $FeCl_2 \cdot 4H_2O$ (24 g) was dissolved in H_2O and mixed with 1 mL of concentrated HCl containing 1 g of dissolved Fe powder. The solution was degassed and heated in an oil bath under an Ar atmosphere for 30 min. The solution was filtered while warm, and the pale greenish colored filtrate was evaporated, leaving a pale greenish solid. White $FeCl_2 \cdot 2H_2O$ was obtained upon heating the greenish powder under vacuum at 80 °C for 1 h. This purified ferrous chloride was stored under Ar in an inert atmosphere box.

$[Fe(tpen)](ClO_4)_2 \cdot {}^2/_3H_2O$. A quantity of 0.163 g (1.00 mmol) of $FeCl_2 \cdot 2H_2O$ was dissolved in 10 mL of degassed 1:1 $MeOH/H_2O$ and heated to 50 °C. Tpen (0.43 g, 1.0 mmol) was dissolved in 8 mL of 1:1 $MeOH/H_2O$, degassed, and added to the warm $FeCl_2$ solution. The reaction mixture immediately turned red upon addition of the tpen solution. An aqueous solution of $NaClO_4$ (0.3 g in 10 mL) was then added slowly to the reaction mixture. The hot solution was allowed to cool to room temperature. A brownish-red microcrystalline solid was retrieved by filtration, washed with cold water, and dried in air. Anal. Calcd for $FeC_{26}H_{29.33}N_6O_{8.67}Cl_2$: C, 45.16; H, 4.13; N, 12.15; Fe, 8.10. Found:

(7) (a) Gütlich, P. In *Chemical Mössbauer Spectroscopy*; Herber, R. H., Ed.; Plenum Press: New York, 1984. (b) Gütlich, P. In *Mössbauer Spectroscopy Applied to Inorganic Chemistry*; Ong, G. J., Ed.; Plenum Press: New York, 1984; Vol. 1. (c) Martin, R. L.; White, A. H. *Trans. Metal. Chem.* **1969**, *5*, 113. (d) Goodwin, H. A. *Coord. Chem. Rev.* **1976**, *18*, 293. (e) Gütlich, P. *Struct. Bond.* **1981**, *44*, 83. (f) Kõnig, E.; Ritter, G.; Kulshrestha, S. K. *Chem. Rev.* **1985**, *85*, 219. (g) Beattie, J. K. *Adv. Inorg. Chem.* **1988**, *32*, 2. (h) Toftlund, H. *Coord. Chem. Rev.* **1989**, *94*, 67.

(8) (a) Dose, E. V.; Hoselton, M. A.; Sutin, N.; Tweedle, M. F.; Wilson, L. J. *J. Am. Chem. Soc.* **1978**, *100*, 1141. (b) Slichter, C. P.; Drickamer, H. G. *J. Chem. Phys.* **1972**, *56*, 2142. (c) Chesnut, D. B. *J. Chem. Phys.* **1964**, *40*, 405. (d) Kambara, T. *J. Chem. Phys.* **1979**, *70*, 4199. (e) Sorai, M.; Seki, S. *J. Phys. Chem. Solids* **1974**, *35*, 555. (f) Wajnflasz, J. *Phys. Stat. Sol.* **1970**, *40*, 537. (g) Bari, R. A.; Sivardiere, J. *Phys. Rev. B* **1972**, *5*, 4466. (h) Ramasesha, S.; Ramakrishnan, T. V.; Rao, C. N. R. *J. Phys. C (Solid State Phys.)* **1979**, *12*, 1307. (i) Hopfield, J. L. *Proc. Natl. Acad. Sci. U.S.A.* **1974**, *71*, 3640. (j) Buhks, E.; Havon, G.; Bixon, M.; Jortner, J. *J. Am. Chem. Soc.* **1980**, *102*, 2918. (k) Sasaki, N.; Kambara, T. *J. Phys. Soc. Jpn.* **1987**, *56(11)*, 3956.

(9) Careri, G. *Order and Disorder in Matter*; Benjamin/Cummings Publishing Co.: Menlo Park, 1984.

(10) (a) Decurtins, S.; Gütlich, P.; Köhler, C. P.; Spiering, H.; Hauser, A. *Chem. Phys. Lett.* **1984**, *105*, 1. (b) Decurtins, S.; Gütlich, P.; Köhler, C. P.; Spiering, H. *J. Chem. Soc., Chem. Commun.* **1985**, 430. (c) Decurtins, S.; Gütlich, P.; Hasselbach, K. M.; Hauser, A.; Spiering, H. *Inorg. Chem.* **1985**, *24*, 2174.

(11) Herber, R. H. *Inorg. Chem.* **1987**, *26*, 173.

(12) Hauser, A.; Adler, J.; Gütlich, P. *Chem. Phys. Lett.* **1988**, *152*, 468.

(13) (a) Dewey, T. G.; Turner, D. H. *Adv. Mol. Relax. Interact. Proc.* **1978**, *13*, 331. (b) Beattie, J. K.; Sutin, N.; Turner, D. H.; Flynn, G. W. *J. Am. Chem. Soc.* **1973**, *95*, 2052. (c) Hoselton, M. A.; Drago, R. S.; Wilson, L. J.; Sutin, N. *J. Am. Chem. Soc.* **1976**, *98*, 6979. (d) Reeder, K. A.; Dose, E. V.; Wilson, L. J. *Inorg. Chem.* **1978**, *17*, 1071.

(14) (a) Beattie, J. K.; Binstead, R. A.; West, R. J. *J. Am. Chem. Soc.* **1978**, *100*, 3044. (b) Binstead, R. A.; Beattie, J. K.; Dose, E. V.; Tweedle, M. F.; Wilson, L. J. *J. Am. Chem. Soc.* **1978**, *100*, 5609. (c) Binstead, R. A.; Beattie, J. K.; Dewey, T. G.; Turner, D. H. *J. Am. Chem. Soc.* **1980**, *102*, 6442. (d) Beattie, J. K.; McMahon, K. J. *Aust. J. Chem.* **1988**, *41(9)*, 1315.

(15) (a) Xie, C.-L.; Hendrickson, D. N. *J. Am. Chem. Soc.* **1987**, *109*, 6981. (b) Conti, A. J.; Xie, C.-L.; Hendrickson, D. N. *J. Am. Chem. Soc.* **1989**, *111*, 1171.

(16) (a) Augustine, R. L.; Van Peppen, J. F. *J. Chem. Soc., Chem. Commun.* **1970**, 497. (b) Purcell, K. F. *J. Am. Chem. Soc.* **1979**, *101*, 5147 and references therein.

(17) Toftlund, H.; Yde-Andersen, S. *Acta Chem. Scand.* **1981**, *A35*, 575.

C, 45.10; H, 4.15; N, 12.18; Fe, 8.12. The orange-red rhomboid single crystal for the X-ray structure determination was obtained by evaporation in air of a 1:1 MeOH/H_2O solution of the complex for a period of 1 day.

[Fe(tpen)](ClO_4)$_2$. A portion of [Fe(tpen)](ClO_4)$_2$·$^2/_3H_2O$ was dissolved in degassed 1:1 MeOH/H_2O and then slowly evaporated under an Ar atmosphere. A mixture of red cube-like crystals and needle-shaped crystals (~10% in the needle morphology) was obtained after 1 week. The cube-like crystals were found to be of X-ray diffraction quality. Anal. Calcd for $FeC_{26}H_{28}N_6O_8Cl_2$: C, 45.97; H, 4.15; N, 12.37; Fe, 8.22. Found: C, 46.05; H, 4.13; N, 12.18; Fe, 8.16.

^{57}Fe-Enriched Samples. A sample of [Fe(tpen)](ClO_4)$_2$·$^2/_3H_2O$ enriched to 50% in ^{57}Fe was prepared by first dissolving 25 mg (0.45 mmol) of 99%-enriched ^{57}Fe powder (New England Nuclear) and 25 mg (0.45 mmol) of unenriched Fe powder in 8 mL of concentrated HCl at 50 °C for 5 min. The resulting pale yellowish solution was evaporated under reduced pressure to give a nearly pure white powder, which was dissolved in 5 mL of a degassed 1:1 MeOH/H_2O solution. Tpen (0.43 g, 1.0 mmol) dissolved in 5 mL of degassed MeOH was then transferred under Ar to the $FeCl_2$ solution. The resulting red solution was stirred and heated for 15 min at 50 °C. An aqueous solution of $NaClO_4$ (0.31 g in 5 mL) was then added to the reaction mixture. A brownish-red microcrystalline product was retrieved by filtration from the cooled solution. The spectroscopic and magnetic properties of this enriched sample were found to be identical with those of the unenriched sample.

[Fe(tpen)]I_2. A quantity of 0.278 g (1.00 mmol) of $FeSO_4$·$7H_2O$ was dissolved in 10 mL of degassed water. Tpen (0.43 g, 1.0 mmol) dissolved in 5 mL of methanol was added to the $FeSO_4$ solution. An aqueous solution of KI (0.5 g in 3 mL) was added slowly to the reaction mixture. A deep red crystalline solid was retrieved by filtration, washed with cold water, and dried in air. Anal. Calcd for $FeC_{26}H_{28}N_6I_2$: C, 42.53; H, 3.84; N, 11.45. Found: C, 42.74; H, 3.86; N, 11.51.

Additional Salts of [Fe(tpen)]$^{2+}$. The BPh_4^-, PF_6^-, and $CF_3SO_3^-$ salts of [Fe(tpen)]$^{2+}$ were all made analogously to the $NaClO_4$ salt, employing solutions of 0.8 g of $NaBPh_4$, 0.3 g of $NaPF_6$, or 0.5 g of $NaCF_3SO_3$. Anal. Calcd for $FeC_{74}H_{68}N_6B_2$: C, 79.47; H, 6.09; N, 7.52; Fe, 5.00. Found: C, 79.49; H, 6.11; N, 7.50; Fe, 4.98. Calcd for $FeC_{26}H_{32}N_6O_3P_2F_{12}$: C, 37.88; H, 4.16; N, 10.19; Fe, 6.79; P, 7.51. Found: C, 38.06; H, 4.24; N, 10.35; Fe, 6.39; P, 7.54. Calcd for $FeC_{28}H_{28}N_6O_6S_2F_6$: C, 43.20; H, 3.13; N, 10.79; Fe, 7.17; S, 8.24. Found: C, 42.63; H, 3.59; N, 10.66; Fe, 7.16; S, 7.85.

[Zn(tpen)](ClO_4)$_2$·$^2/_3H_2O$. The procedure used to prepare this compound was similar to that of the ferrous complex, except that the Zn reaction was done in air. The reaction of $ZnCl_2$ with tpen produced a white microcrystalline product that was recrystallized from a 1:5 EtOH/H_2O solution. Anal. Calcd for $ZnC_{26}H_{29.33}N_6O_{8.67}Cl_2$: C, 44.56; H, 4.22; N, 11.99; Zn, 9.33. Found: C, 44.36; H, 4.20; N, 12.22; Zn, 9.26.

[Fe_xZn_{1-x}(tpen)](ClO_4)$_2$·$^2/_3H_2O$ (x = 0.1, 0.2, 0.5, 0.7). This series of diluted compound was prepared by mixing the appropriate molar ratios of [Fe(tpen)](ClO_4)$_2$·$^2/_3H_2O$ and [Zn(tpen)](ClO_4)$_2$·$^2/_3H_2O$ in 10 mL of 1:1 MeOH/H_2O under argon. $NaClO_4$ was added to the stirring solution to ensure the homogeneity of the product. The retrieved solids were isolated by filtration, washed, and dried as described above. Results of the elemental analyses for these compounds are available in the supplementary material.

Physical Measurements. Variable-Temperature Magnetic Susceptibility. Magnetic susceptibility data were collected on a VTS-50 Series 800 SQUID type susceptometer (S.H.E. Corp.) interfaced to an Apple II+ computer. The sample was packed in a cylindrical Delrin sample container with an inner diameter of approximately 4 mm. Sample temperature control was achieved using a S.H.E. digital temperature device. Each data point was taken as the average of five samplings after the sample had reached thermal equilibrium. A magnetic field of 10 kG was used. For all the data reported, diamagnetic corrections estimated from Pascal's constants[18] were applied in determining the molar paramagnetic susceptibility of the compound.

Magnetic susceptibility measurements for solutions of spin-crossover complexes were carried out by the Faraday technique employing an electromagnet (Bruker Physik), an electromicrobalance (Satorius Model 411), and a temperature controller (BVT Model 1000). Airtight aluminum sample tubes were filled under argon. Calibrations were performed against the actual solvent used in each case.

^{57}Fe Mössbauer Spectroscopy. ^{57}Fe Mössbauer spectra were collected with use of a previously described vertical-drive transmission spectrometer operating in the constant-acceleration mode.[19] Sample temperatures were controlled with a Lake Shore Cryogenics Model DRC 80C temperature controller in conjunction with a Si diode mounted on a copper sample holder. A copper–constantan thermocouple and a Yellow Springs Instrument 44003A precision thermistor, both mounted on the sample holder, were used to monitor the sample temperature. The absolute precision is estimated to be ±3 K; the relative precision was approximately 0.5 K. Spectra were fit to Lorentzian line shapes by using a previously described computer program.[20] Isomer shifts are reported relative to natural iron foil at 300 K. No temperature-dependent second-order Doppler shift corrections were applied.

Table I. Crystallographic Data for [Fe(tpen)](ClO_4)$_2$·nH_2O

	n = 0	n = $^2/_3$	
formula	$FeCl_2O_8N_6C_{26}H_{28}$	$FeCl_2O_{8.67}N_6C_{26}H_{29.33}$	
formula wt	679.299	691.309	
cryst size, mm	0.2 × 0.3 × 0.3	0.2 × 0.3 × 0.9	
temp, K	298	298	358
space group	$P2_1/c$ (No. 14)	$C2/c$ (No. 15)	$C2/c$ (No. 15)
a, Å	17.865 (3)	40.87 (2)	41.00 (2)
b, Å	9.878 (1)	9.497 (4)	9.517 (5)
c, Å	17.213 (4)	23.946 (9)	24.21 (1)
β, deg	110.01 (2)	108.42 (4)	109.46 (4)
V, Å^3	2854 (2)	8819 (14)	8905 (15)
Z	4	12	12
ρ_{calc}, g cm^{-3}	1.581	1.562	1.547
λ(Kα), Å	0.71073	0.71073	0.71073
2θ range, deg	2.0–53.0	2.0–48.0	2.0–48.0
octants collected	$\pm h, -k, +l$	$\pm h, +k, +l$	$\pm h, +k, -l$
total reflcns	5905	6898	6961
obsd reflcns[a]	3031	3110	2221
μ, cm^{-1}	7.73	7.54	7.46
R^b	0.049	0.073	0.082
R_w^c	0.053	0.076	0.082

[a] $I > 2.58\sigma(I)$. [b] $R = \sum(|F_o| - |F_c|)/\sum|F_o|$. [c] $R_w = [\sum w(|F_o| - |F_c|)^2/[\sum w|F_o|^2]^{1/2}$.

Electronic Spectra. Variable-temperature electronic absorption spectra were recorded on a Hewlett Packard Model 8452A diode array spectrophotometer. Temperature control was achieved with a Hewlett Packard Model 89054A thermostated cell holder, connected to a Fisher Scientific Model 800 Isotemp circulating bath. Temperature stability was better than ±0.3 K; the absolute accuracy is estimated at ±1 K. Measurements were carried out in HPLC-grade H_2O at 1.88 × 10^{-4} m. Each spectrum represents a signal average of 250 individual spectra taken at 0.1-s intervals after the solution had equilibrated for 15 min. Spectral changes were found to be reversible at this concentration, as cooling the solution from 363 K to ambient temperature resulted in better than 99% recovery of the starting spectrum.

X-ray Structure Determination. All three of the single-crystal structure determinations were carried out at the crystallographic center of the Department of Chemistry, University of Illinois. Diffraction data were collected on an Enraf-Nonius CAD4 automated k-axis diffractometer equipped with a graphite crystal monochromator. The ω/θ scan technique was used to record the intensities for all nonequivalent reflections. Scan widths were calculated as $A + B \tan\theta$, where A is estimated from the mosaicity of the crystal and B allows for the increase in peak width due to Mo Kα_1 – Kα_2 splitting.

Data were collected for [Fe(tpen)](ClO_4)$_2$ at 25 °C and at both 25 and 85 °C for [Fe(tpen)](ClO_4)$_2$·$^2/_3H_2O$. Pertinent details regarding the structure determinations are listed in Table I for all three structures. The unit cell parameters were obtained by a least-squares fit to the automatically centered settings from 25 reflections. The space group was unambiguously determined from systematic conditions for the nonsolvated structure. The space group confirmation for the solvated compound was based upon the average values of the normalized structure factors and the successful refinement of the proposed model in the centric space group. The intensities from three standard reflections for each measurement showed no significant fluctuation during data collection. Intensity data for all three structures were corrected for Lorentz and polarization effects, as well as anomalous dispersion effects. Absorption corrections were applied for all three data sets. No ψ scans were collected.

The structure of the nonsolvated complex was solved by Patterson methods; the correct position for the iron atom was deduced from a weighted Patterson map. Two consecutive weighted Fourier syntheses revealed positions for the remaining non-hydrogen atoms. In the final

(18) Boudreaux, E. A.; Mulay, L. N., Eds. *Theory and Applications of Molecular Paramagnetism*; John Wiley and Sons: New York, 1976.

(19) Cohn, M. J.; Timken, M. D.; Hendrickson, D. N. *J. Am. Chem. Soc.* **1984**, *106*, 6683.

(20) Chrisman, B. L.; Tumollio, T. A. *Comput. Phys. Commun.* **1971**, *2*, 322.

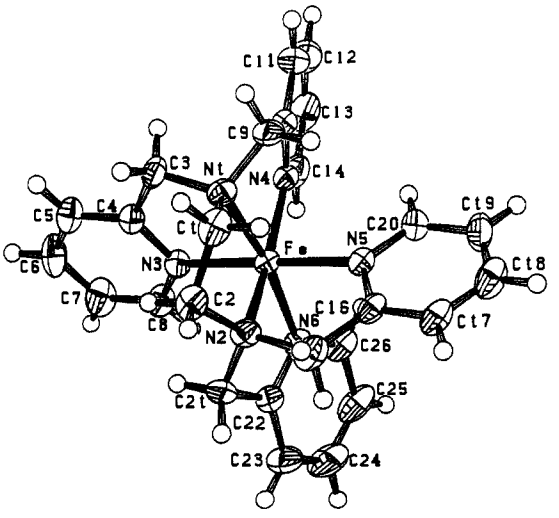

Figure 1. ORTEP drawing of the $[Fe(tpen)]^{2+}$ cation found in $P2_1/c$ symmetry $[Fe(tpen)](ClO_4)_2$.

cycle of least squares, all non-hydrogen atoms were refined with anisotropic thermal coefficients that were fixed in "idealized" positions, and an empirical isotropic extinction coefficient was refined. Successful convergence was indicated by the maximum shift/error for the last cycle. The final difference Fourier map had no residual density that was significantly above the background, and the highest peaks in the map appeared to represent minor disorders (less than 10% occupancy) about the two chlorine atoms. There were no significant features in the final map to indicate the presence of solvent molecules in the lattice. There were no systematic errors among the observed and calculated structure factors; only 6 of 3031 reflections had values for $|F_o - F_c|/\sigma(F_o) > 3$.

The structure for the solvated compound at room temperature was solved by direct methods, SHELXS-86; correct positions for all non-hydrogen atoms excluding the chlorine and oxygen atoms from the two disordered perchlorate molecules were deduced from an E-map. Subsequent least-squares difference Fourier calculations revealed severely disordered positions for two of the perchlorate ions. Unsuccessful attempts to refine independent positions for partially occupied oxygen atom positions suggested disordered positions for the chlorine atoms. "Idealized" perchlorate molecules were refined as rigid groups, three sites for the ion centered on Cl2 [relative site occupancies 0.373 (5), 0.420 (5), and 0.207 (10) for A, B, and C groups, respectively] and four for the Cl3 ion [0.262 (4), 0.162 (2), 0.346 (5), and 0.103 (2)]. Hydrogen atoms were included as fixed contributors in "idealized" positions. In the final cycle of least squares, one group isotropic thermal parameter was refined for hydrogen atoms and one each for the two disordered perchlorate molecules; independent isotropic thermal coefficients were refined for the carbon atoms and the remaining atoms were refined with anisotropic thermal coefficients. The final difference Fourier map had no significant features. A final analysis of variance between observed and calculated structure factors showed no apparent systematic errors.

The high-temperature structure of the solvated form was solved by correlation to the room temperature structure. The two most prominent structural differences between the low- and high-temperature models involved the disorder of one of the perchlorates and the disappearance of the water solvate molecule for the latter. "Idealized" perchlorate molecules were refined as rigid groups: three sites for the ion centered on Cl1 [relative site occupancies 0.35 (1), 0.36 (1), and 0.29 (1) for groups A, B, and C, respectively], and four sites for Cl3 [0.23 (1), 0.16 (1), 0.32 (1), and 0.29 (1)]. Hydrogen atoms were included as fixed contributors in "idealized" positions. In the final cycle of least squares, one group isotropic thermal parameter was refined for the hydrogen atoms and one each for the three disordered perchlorate molecules, and the iron atoms were refined with anisotropic thermal coefficients. The final difference Fourier map had no significant features; there was no evidence of the water molecule located for the room temperature refinement. A final analysis of variance between observed and calculated structure factors showed no apparent systematic errors.

Results and Discussion

X-ray Crystal Structure of $[Fe(tpen)](ClO_4)_2$. The nonsolvated form of this compound crystallizes in the monoclinic space group $P2_1/c$. Final positional parameters are given in Table II; selected bond distances and angles are given in Table III. A computer drawing of the complex ion $[Fe(tpen)]^{2+}$ is given in Figure 1. The

Table II. Positional Parameters for $P2_1/c$ Symmetry $[Fe(tpen)](ClO_4)_2$[a]

	x/a	y/b	z/c
Fe	0.24042 (4)	0.16727 (7)	0.14734 (4)
ClA	0.04142 (8)	−0.3455 (2)	0.18241 (8)
ClB	0.58269 (9)	0.2017 (2)	0.3808 (1)
O1	0.1110 (3)	−0.4040 (6)	0.2359 (3)
O2	0.0109 (3)	−0.2508 (5)	0.2247 (3)
O3	0.0549 (3)	−0.2827 (6)	0.1172 (3)
O4	−0.0167 (3)	−0.4459 (5)	0.1481 (3)
O5	0.6583 (3)	0.1472 (6)	0.4030 (5)
O6	0.5290 (4)	0.1023 (7)	0.3678 (5)
O7	0.5702 (5)	0.2806 (7)	0.3120 (4)
O8	0.5791 (3)	0.2902 (6)	0.4463 (3)
N1	0.1508 (2)	0.1885 (4)	0.1913 (2)
N2	0.1797 (2)	0.2930 (4)	0.0570 (3)
N3	0.2916 (2)	0.3116 (4)	0.2283 (2)
N4	0.2755 (3)	0.0338 (4)	0.2392 (2)
N5	0.1904 (2)	0.0231 (4)	0.0652 (2)
N6	0.3206 (2)	0.1868 (4)	0.0914 (2)
C1	0.0845 (3)	0.2514 (6)	0.1245 (3)
C2	0.1195 (3)	0.3611 (6)	0.0858 (3)
C3	0.1758 (3)	0.2758 (5)	0.2668 (3)
C4	0.2507 (3)	0.3509 (5)	0.2777 (3)
C5	0.2781 (3)	0.4498 (6)	0.3358 (3)
C6	0.3504 (4)	0.5100 (6)	0.3470 (4)
C7	0.3926 (3)	0.4684 (7)	0.2990 (4)
C8	0.3631 (3)	0.3693 (6)	0.2412 (3)
C9	0.1348 (3)	0.0498 (6)	0.2145 (3)
C10	0.2139 (3)	−0.0111 (5)	0.2614 (3)
C11	0.2259 (5)	−0.0998 (6)	0.3262 (4)
C12	0.3001 (6)	−0.1458 (7)	0.3676 (4)
C13	0.3628 (5)	−0.1001 (7)	0.3469 (4)
C14	0.3493 (3)	−0.0099 (6)	0.2818 (3)
C15	0.1400 (3)	0.2170 (6)	−0.0207 (3)
C16	0.1450 (3)	0.0688 (6)	−0.0099 (3)
C17	0.1090 (3)	−0.0183 (7)	−0.0747 (3)
C18	0.1203 (3)	−0.1530 (8)	−0.0639 (4)
C19	0.1680 (4)	−0.2013 (6)	0.0114 (4)
C20	0.2022 (3)	−0.1114 (6)	0.0743 (3)
C21	0.2405 (3)	0.3861 (5)	0.0454 (3)
C22	0.3091 (3)	0.2998 (6)	0.0451 (3)
C23	0.3579 (4)	0.3315 (7)	0.0006 (4)
C24	0.4190 (4)	0.2471 (9)	0.0031 (4)
C25	0.4285 (3)	0.1319 (8)	0.0476 (4)
C26	0.3794 (3)	0.1022 (6)	0.0920 (3)

[a] Estimated standard deviations for the last significant figure are given in parentheses. Hydrogen atom positions were calculated, see supplementary material.

structure of the Co^{III} complex of this ligand has very recently been reported.[21] The $[Fe(tpen)]^{2+}$ complex ion has a distorted octahedral coordination geometry, with two aliphatic (N1 and N2) and four aromatic (N3–N6) nitrogen atoms comprising the N_6 coordination sphere. Due to the puckering of the ethylenediamine ring, the Fe–N1–N2–N4–N6 coordination plane is not strictly planar, but exhibits a tilt of 4.4°. The chelate rings of the picolylamine also exhibit deviations from planarity. The 2-pyridylmethyl groups are planar as expected, but are tilted with respect to the coordination plane, resulting in average torsional N–C–C–N angles of 30.5° for the pyridylamine fragments. The combination of these tilts causes the observed dihedral angles of 20.1° and 17.3° between the N1–Fe–N2 plane and the pyridine planes. This helical arrangement reduces the steric interactions between pyridine hydrogen atoms in the 6-position in a given plane (e.g., H14 and H26). The pyridine planes themselves are nearly perpendicular to each other.

The fusion of the five-membered chelate rings and the ethylenediamine linkage result in marked deviations from octahedral symmetry. If we define the two trigonal planes according to the geometry of the ligand itself, that is, one plane as N1–N3–N4 and the other as N2–N5–N6, two different types of trigonal angles are identified. The average trigonal twist of type I (A, B, and

(21) Mandel, J. B.; Douglas, B. E. *Inorg. Chim. Acta* **1989**, *155*, 55.

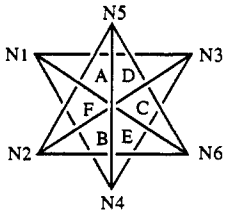

C) is found to be 49.5°. For the type II trigonal twist (D, E, and F), the average angle is 70.5°. These are to be compared with the expected twist of 60° for a strictly octahedral complex. This substantial trigonal distortion (ϕ = 10.5°) is reflected in the strained N4–Fe–N1 and N2–Fe–N6 angles of 81.0 (2)° and 81.5 (2)°, respectively, which cause the N4–Fe–N6 angle to expand to 111.5 (2)°. However, all four Fe–N_{py} distances are virtually identical to within 0.002 Å at 1.988 Å (av) and the two Fe–N_{aliph} distances are statistically identical [2.002 (4) Å for Fe–N1; 1.996 (4) Å for Fe–N2]. The slightly shorter Fe–N_{py} distances are possibly due to some degree of π-back-bonding between the Fe center and the pyridine rings. All of these bond distances are consistent with those observed for several other low-spin ferrous complexes.[22] The results from magnetic studies further establish the low-spin configuration of $[Fe(tpen)](ClO_4)_2$ at room temperature (vide infra). The molecule as a whole has only C_1 symmetry; however, the ligand field can be reasonably approximated as C_{2v}.

X-ray Crystal Structures of $[Fe(tpen)](ClO_4)_2 \cdot {}^2/_3H_2O$. The solvated form of $[Fe(tpen)](ClO_4)_2$ crystallizes in the monoclinic space group $C2/c$ at 25 °C. Final positional parameters for the structure are given in Table IV; selected bond distances and angles are listed in Table V. Crystallographically, the cation occupies two different sites in the lattice (herein defined as site A and site B). Site A occurs as a general position, whereas molecules at site B sit at special positions in the $C2/c$ unit cell. These positions exist in a 2:1 ratio in the lattice, and analyses of spectroscopic data (e.g., ^{57}Fe Mossbauer, vide infra) must take this distinction into account. The two molecular types, in addition to sitting at different crystallographic positions, exhibit slightly different structural characteristics. Both complexes possess distorted octahedral geometries, similar in nature to those described for the nonsolvated form (vide supra). The degree of distortion due to the puckering of the ethylenediamine linkage is substantially different, with tetragonal twists of 5.5° and 2.3° for cations in sites A and B, respectively. Both of these values are to be compared with the 4.4° twist found for the unsolvated complex. Deviations from the plane of coordination for the pyridine rings are also noted. The dihedral angles produced are somewhat smaller than those noted for the unsolvated form: 17.9° and 18.7° for site A; 15.2° and 19.5° for site B.

The trigonal twist angles are also quite different for the two sites at 25 °C. The average type I angle (vide supra) for site A is 45.7°, while for site B molecules this average is 49.5° (i.e., the degree of distortion ϕ is 14.8° for site A and 10.5° for site B). Similar differences are noted in the values for the type II angles: 74.3° for site A and 70.4° for site B. It is clear that the degree of trigonal distortion is larger for the site A molecules than for the site B molecules.

The Fe–N bond distances for each site require some comment. The average Fe–N_{py} distance is found to be identical for both sites at 2.02 (1) Å. However, the Fe–N_{aliph} distances are significantly different: 2.03 (1) Å for site A, compared to 1.98 (1) Å for site B molecules. The bond distances for the site B molecules compare well with the corresponding values for the nonsolvated complex. The longer amine distance for site A suggests a contribution from the small fraction of high-spin component present at room temperature for the solvated complex (vide infra). It should be noted, however, that the strikingly similar bond distances noted in the $P2_1/c$ structure for the groups of two aliphatic and four pyridine nitrogens are not found in this structure. For site A, the Fe–N1 and Fe–N2 distances are 2.022 (8) and 2.044 (8) Å, respectively. Variations for the Fe–N_{py} distances are even larger, with distances ranging from 1.977 (8) to 2.046 (8) Å. It is interesting that only the site A molecules reflect the high-spin component in this system at 25 °C. There is no obvious difference in intermolecular contacts for cations at site A compared to those at site B, which is evident from the packing diagram (Figure 2). Furthermore, an analysis of van der Waals contacts indicates that each cation is essentially isolated in the lattice. It is possible that the influence of the solvate molecule (indicated in the packing diagram as lone ellipses) is different for the two different sites in the lattice. It is well-established that solvate molecules can have a dramatic impact on spin-crossover properties.[7e,f]

In addition, it is interesting to note in this context that the degree of trigonal distortion is larger at site A than at site B (vide supra). Bond distances at site B correspond quite well with the unsolvated structure, all low spin at this temperature, as do the values for the trigonal twist angles. Site A, which reflects the portion of high-spin component present at this temperature based on Fe–N bond distances, also has a greater degree of trigonal distortion. This correlation between trigonal distortion and the presence of high-spin species is further established with the higher temperature structure (vide infra).

The crystal structure of the solvated form of $[Fe(tpen)](ClO_4)_2$ was also determined at 85 °C in an effort to see what structural changes accompany the spin-state transformation. Such information is extremely valuable in understanding the vibronic nature of the spin-crossover phenomenon, but good structures of both the high-spin and low-spin form of a single complex have only been possible in a few cases for ferrous systems.[23] Even in the present work, the high-temperature structure represents only a contribution from the high-spin form; the T_c (n_{HS} = 0.50) is approximately 365 K for $[Fe(tpen)](ClO_4)_2 \cdot {}^2/_3H_2O$ (vide infra). However, substantial changes were noted in the structural parameters for the compound. Table VI contains positional parameters for the high-temperature structure, and Table VII contains selected bond distances and angles. Most obvious are the changes in the Fe–N bond distances. Both the Fe–N_{py} and Fe–N_{aliph} distances are found to increase with an increase in the high-spin fraction. Again, a difference between site A and site B molecules is observed: the average Fe–N_{py} distance at site A is 2.06 (1) Å, while this distance is 2.09 (1) Å at site B; the Fe–N_{aliph} bond length is 2.09 (1) Å at site A, but only 2.04 (2) Å at site B. This latter observation is in accord with the observations made for the room temperature structure, in that the amine distance at site A seems to reflect more prominently the presence of the high-spin fraction. In addition, the variation in bond length within the Fe–N_{py} bond type, in particular, is much more pronounced in the high-temperature structure (Fe–N4 at 2.01 (1) Å compared to Fe–N5 at 2.12 (1) Å). The bond distances for Fe–N1 and Fe–N2 are identical to within the accuracy of the structure (2.01 (1) Å). The reason for the longer average Fe–N_{py} distance at site B is not clear, but it may reflect in part the large disparity among the individual bond distances. It is interesting to note that the variance of the individual Fe–N bond distances appears to become more pronounced with increasing contribution from the high-spin species (i.e., unsolvated form → solvated, 25 °C → solvated, 85 °C (vide infra)).

With such large changes in bond distances, it is not surprising that there are substantial differences in the various bond angles between the room and high temperature structures for the solvate. The tetragonal twist for the A and B molecules is larger in both cases at 85 °C at 8.1° and 6.3°, respectively. The average torsional angle associated with the picolylamine ring also increases, from 30.0° at room temperature to 31.5° at 85 °C. The trigonal twist angles indicate that the higher temperature structure is even more

(22) König, E. *Prog. Inorg. Chem.* **1987**, *35*, 527.

(23) (a) Greenway, A. M.; Sinn, E. J. *J. Am. Chem. Soc.* **1978**, *100*, 8080. (b) Greenway, A. M.; O'Connor, C. J.; Schrock, A.; Sinn, E. *Inorg. Chem.* **1979**, *18*, 2692. (c) Katz, B. A.; Strouse, C. E. *Inorg. Chem.* **1980**, *19*, 658. (d) Oliver, J. D.; Mullica, D. F.; Hutchinson, B. B.; Milligan, W. O. *Inorg. Chem.* **1980**, *19*, 165. (e) Cecconi, F.; Di Vaira, M.; Midollini, S.; Orlandini, A.; Sacconi, L. *Inorg. Chem.* **1981**, *20*, 3423.

Table III. Selected Bond Distances and Angles for $P2_1/c$ Symmetry $[Fe(tpen)](ClO_4)_2$[a]

		Distances, Å			
ClA–O1	1.394 (6)	ClA–O2	1.404 (5)	ClA–O3	1.374 (5)
ClA–O4	1.411 (6)	ClB–O5	1.381 (5)	ClB–O6	1.336 (7)
ClB–O7	1.371 (6)	ClB–O8	1.446 (6)	Fe–N1	2.002 (4)
Fe–N2	1.996 (4)	Fe–N3	1.984 (4)	Fe–N4	1.987 (4)
Fe–N5	1.990 (4)	Fe–N6	1.990 (4)	N1–C1	1.476 (6)
N2–C2	1.491 (7)	C1–C2	1.514 (8)	N1–C3	1.495 (6)
N3–C4	1.354 (6)	C3–C4	1.485 (7)	C4–C5	1.364 (7)
C5–C6	1.375 (8)	C6–C7	1.358 (9)	N3–C8	1.345 (6)
C7–C8	1.366 (8)	N1–C9	1.482 (7)	N4–C10	1.358 (7)
C9–C10	1.494 (8)	C10–C11	1.376 (8)	C11–C12	1.35 (1)
C12–C13	1.36 (1)	N4–C14	1.343 (7)	C13–C14	1.387 (8)
N2–C15	1.485 (7)	N5–C16	1.347 (6)	C15–C16	1.475 (8)
C16–C17	1.381 (8)	C17–C18	1.35 (1)	C18–C19	1.370 (9)
N5–C20	1.346 (7)	C19–C20	1.372 (8)	N2–C21	1.488 (7)
N6–C22	1.346 (7)	C21–C22	1.494 (8)	C22–C23	1.379 (8)
C23–C24	1.36 (1)	C24–C25	1.35 (1)	N6–C26	1.340 (7)
C25–C26	1.377 (8)				
		Angles, deg			
N1–Fe–N2	86.4 (2)	N1–Fe–N3	84.0 (2)	N1–Fe–N4	81.0 (2)
N1–Fe–N5	96.9 (2)	N1–Fe–N6	166.8 (2)	N2–Fe–N3	95.6 (2)
N2–Fe–N4	166.3 (2)	N2–Fe–N5	84.2 (2)	N2–Fe–N6	81.5 (2)
N3–Fe–N4	88.5 (2)	N3–Fe–N5	179.0 (2)	N3–Fe–N6	92.0 (2)
N4–Fe–N5	91.9 (2)	N4–Fe–N6	111.5 (2)	N5–Fe–N6	87.1 (2)
O1–ClA–O2	110.5 (3)	O1–ClA–O3	111.1 (3)	O1–ClA–O4	110.4 (3)
O2–ClA–O3	109.3 (3)	O2–ClA–O4	109.0 (3)	O3–ClA–O4	106.5 (3)
O5–ClB–O6	109.7 (4)	O5–ClB–O7	108.4 (5)	O5–ClB–O8	108.7 (4)
O6–ClB–O7	112.2 (5)	O6–ClB–O8	110.8 (4)	O7–ClB–O8	107.0 (4)
Fe–N1–C1	106.4 (3)	Fe–N1–C3	110.4 (3)	Fe–N1–C9	105.0 (3)
C1–N1–C3	110.8 (4)	C1–N1–C9	114.9 (4)	C3–N1–C9	109.1 (4)
Fe–N2–C2	106.4 (3)	Fe–N2–C15	110.6 (3)	Fe–N2–C21	105.2 (3)
C2–N2–C15	110.5 (4)	C2–N2–C21	114.2 (4)	C15–N2–C21	109.7 (4)
Fe–N3–C4	115.4 (3)	Fe–N3–C8	127.2 (3)	C4–N3–C8	117.4 (4)
Fe–N4–C10	112.1 (3)	Fe–N4–C14	129.1 (4)	C10–N4–C14	118.7 (4)
Fe–N5–C16	114.7 (3)	Fe–N5–C20	127.5 (3)	C16–N5–C20	117.5 (4)
Fe–N6–C22	112.2 (3)	Fe–N6–C26	128.9 (4)	C22–N6–C26	118.8 (4)
N1–C1–C2	107.5 (4)	N2–C2–C1	106.1 (4)	N1–C3–C4	112.7 (4)
N3–C4–C3	115.7 (4)	N3–C4–C5	122.1 (4)	C3–C4–C5	122.2 (4)
C4–C5–C6	119.8 (5)	C5–C6–C7	118.3 (6)	C6–C7–C8	120.3 (5)
N3–C8–C7	122.2 (5)	N1–C9–C10	106.5 (4)	N4–C10–C9	115.1 (4)
N4–C10–C11	121.3 (6)	C9–C10–C11	123.4 (6)	C10–C11–C12	119.7 (7)
C11–C12–C13	119.8 (7)	C12–C13–C14	119.5 (7)	N4–C14–C13	121.0 (6)
N2–C15–C16	113.5 (4)	N5–C16–C15	116.4 (5)	N5–C16–C17	121.9 (5)
C15–C16–C17	121.7 (5)	C16–C17–C18	119.8 (5)	C17–C18–C19	119.3 (6)
C18–C19–C20	119.1 (6)	N5–C20–C19	122.5 (5)	N2–C21–C22	106.6 (4)
N6–C22–C21	115.5 (5)	N6–C22–C23	121.3 (5)	C21–C22–C23	123.2 (5)
C22–C23–C24	119.7 (6)	C23–C24–C25	118.5 (6)	C24–C25–C26	121.0 (6)
N6–C26–C25	120.6 (5)				

[a] Estimated standard deviations for the last significant figure are given in parentheses.

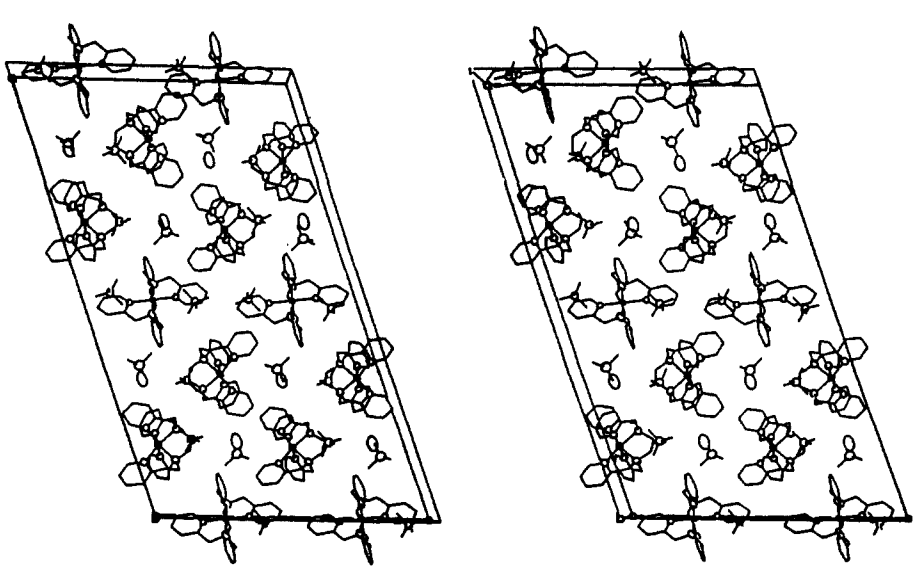

Figure 2. Stereoview of the packing diagram for $C2/c$ symmetry $[Fe(tpen)](ClO_4)_2 \cdot {}^2/_3H_2O$.

distorted along that coordinate: the type I angles are 42.6° and 46.7° for the A and B sites, respectively; the type II angles are found to be 77.4° and 73.3° (ϕ = 17.4° for A, ϕ = 13.3° for B). A comparison of the information in Tables V and VII makes clear

Table IV. Positional Parameters for $C2/c$ Symmetry $[Fe(tpen)](ClO_4)_2 \cdot {}^2/_3H_2O$ at 298 K[a]

	x/a	y/b	z/c
Fe1	0.16658 (4)	−0.2354 (2)	0.59554 (6)
Fe1	0.0	0.1657 (2)	0.75
O	0.3204 (4)	0.307 (2)	0.1191 (5)
Cl1	0.17956 (8)	0.2617 (3)	0.7213 (1)
O1	0.1768 (3)	0.1306 (9)	0.7451 (5)
O2	0.2057 (2)	0.258 (1)	0.6949 (4)
O3	0.1481 (2)	0.299 (1)	0.6800 (4)
O4	0.1877 (3)	0.3637 (10)	0.7666 (4)
N1	0.1337 (2)	−0.2961 (8)	0.6388 (3)
N2	0.2021 (2)	−0.2144 (9)	0.6772 (3)
N3	0.1405 (2)	−0.0518 (8)	0.5873 (3)
N4	0.1282 (2)	−0.2983 (8)	0.5266 (3)
N5	0.1914 (2)	−0.4230 (8)	0.5968 (3)
N6	0.2047 (2)	−0.1442 (9)	0.5725 (3)
N7	0.0360 (2)	0.0123 (9)	0.7715 (3)
N8	0.0068 (2)	0.1650 (9)	0.8363 (3)
N9	0.0415 (2)	0.2831 (8)	0.7651 (3)
C1	0.1552 (3)	−0.330 (1)	0.6992 (5)
C2	0.1825 (3)	−0.217 (1)	0.7186 (5)
C3	0.1096 (3)	−0.180 (1)	0.6403 (5)
C4	0.1121 (3)	−0.056 (1)	0.6041 (5)
C5	0.0877 (3)	0.046 (1)	0.5898 (5)
C6	0.0915 (3)	0.159 (1)	0.5563 (5)
C7	0.1205 (3)	0.163 (1)	0.5384 (5)
C8	0.1446 (3)	0.059 (1)	0.5555 (5)
C9	0.1147 (3)	−0.418 (1)	0.6055 (5)
C10	0.1063 (3)	−0.387 (1)	0.5410 (5)
C11	0.0783 (3)	−0.449 (1)	0.4984 (5)
C12	0.0745 (3)	−0.423 (1)	0.4416 (5)
C13	0.0962 (3)	−0.331 (1)	0.4257 (5)
C14	0.1220 (3)	−0.267 (1)	0.4692 (5)
C15	0.2281 (3)	−0.331 (1)	0.6878 (5)
C16	0.2214 (3)	−0.434 (1)	0.6396 (5)
C17	0.2463 (3)	−0.534 (1)	0.6388 (5)
C18	0.2375 (3)	−0.630 (1)	0.5944 (5)
C19	0.2067 (3)	−0.627 (1)	0.5523 (5)
C20	0.1841 (3)	−0.520 (1)	0.5530 (5)
C21	0.2192 (3)	−0.077 (1)	0.6740 (5)
C22	0.2277 (3)	−0.076 (1)	0.6177 (5)
C23	0.2564 (3)	−0.010 (1)	0.6114 (5)
C24	0.2615 (3)	−0.012 (1)	0.5580 (5)
C25	0.2385 (3)	−0.079 (1)	0.5113 (5)
C26	0.2106 (3)	−0.145 (1)	0.5209 (5)
C27	0.0168 (3)	−0.117 (1)	0.7449 (5)
C28	0.0504 (3)	−0.004 (1)	0.8362 (5)
C29	0.0309 (3)	0.075 (1)	0.8685 (4)
C30	0.0376 (3)	0.059 (1)	0.9292 (5)
C31	0.0206 (3)	0.145 (1)	0.9563 (5)
C32	−0.0025 (3)	0.242 (1)	0.9254 (4)
C33	−0.0086 (2)	0.251 (1)	0.8654 (4)
C34	0.0627 (3)	0.058 (1)	0.7467 (5)
C35	0.0692 (3)	0.209 (1)	0.7604 (5)
C36	0.1001 (3)	0.277 (1)	0.7680 (5)
C37	0.1038 (3)	0.415 (1)	0.7802 (6)
C38	0.0771 (3)	0.492 (2)	0.7872 (5)
C39	0.0453 (3)	0.421 (1)	0.7788 (5)

[a] Estimated standard deviations for the last significant figure are given in parentheses. One perchlorate ion centered at Cl1 was not disordered. Two of the perchlorate ions were found to be disordered and were refined with rigid groups, three sites for the ClO_4^- centered on Cl(2) [relative site occupancies 0.373 (5), 0.420 (5), and 0.207 (10)] and four sties for the ClO_4^- centered on Cl(3) [relative site occupancies 0.262 (4), 0.162 (2), 0.346 (5), and 0.103 (2)]. Positional parameters for these two disordered ClO_4^- ions are available in the supplementary material.

the fact that there are substantial geometric rearrangements associated with the spin-state change *in addition* to the expected increase in Fe–N bond lengths.

Spin-Crossover Properties. Magnetic Susceptibility. The magnetic properties of both the solvated and unsolvated forms of $[Fe(tpen)](ClO_4)_2$ clearly show that both forms undergo a spin-crossover transformation in the temperature region studied. Plots of μ_{eff} versus temperature for the two forms of the complex are given in Figure 3. Both forms have relatively high T_c values,

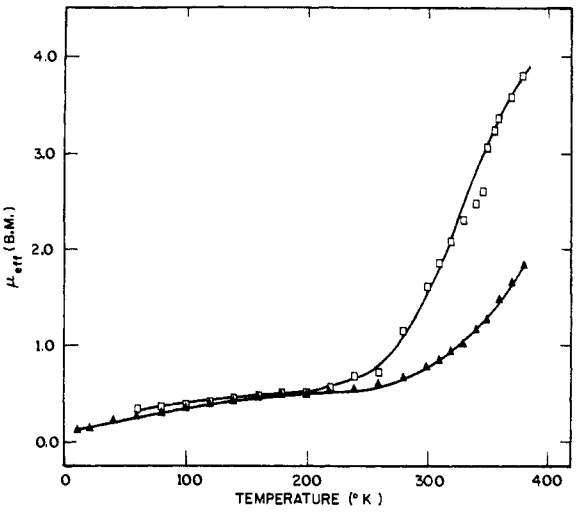

Figure 3. Plot of μ_{eff} versus temperature for $[Fe(tpen)](ClO_4)_2 \cdot nH_2O$; ▲, $n = 0 (P2_1/c)$; □, $n = {}^2/_3 (C2/c)$. (Note: the discontinuity in data for $[Fe(tpen)](ClO_4)_2 \cdot {}^2/_3H_2O$ at ~350 K is an artifact of the susceptometer.)

and in both cases the spin transformation is incomplete at the highest temperatures studied. The fraction of high-spin species present at a given temperature was calculated by using the relation

$$n_{HS} = \{\mu_{eff}^2 - \mu_{eff}^2(LS)\}/\{\mu_{eff}^2(HS) - \mu_{eff}^2(LS)\}$$

assuming a high-spin effective moment of $\mu_{eff} = 4.90$ and a low-spin moment of $\mu_{eff} = 0.00$. The value of n_{HS} for each complex at 380 K is 0.14 for the unsolvated form and 0.60 for the water solvate. A complete listing of n_{HS} for both complexes is given in Tables XS and XIS (supplementary material). From these data, a T_c of approximately 365 K can be interpolated for the solvated complex. The corresponding value for the unsolvated complex is more difficult to estimate, but it certainly lies above 400 K. No thermal hysteresis was observed for either compound.

The reason for this difference in critical temperatures for the two crystalline forms likely comes from a variety of sources. It is well-known that the presence of hydrogen-bonding solvate molecules can have a substantial impact on spin-crossover properties, particularly for complexes of amines.[7e] The lower transition temperature for $[Fe(tpen)](ClO_4)_2 \cdot {}^2/_3H_2O$ suggests a possible interaction between the complex and the solvate molecule. However, such an interaction is not readily distinguishable from the packing diagram (Figure 2) due in part to the fact that the H_2O molecules are undergoing rapid reorientation in the lattice. Alternatively, notwithstanding the presence of a solvate, the different crystal packing of the $P2_1/c$ structure as compared to the $C2/c$ structure of the solvate could change the lattice environment so as to modify the zero-point energy difference between the LS and HS states. These types of phenomena are well-represented in the spin-crossover literature.[7e,f,h,24]

^{57}Fe Mössbauer Spectra. The variable-temperature ^{57}Fe Mössbauer spectra of both the hydrated and nonhydrated forms of $[Fe(tpen)](ClO_4)_2$ were obtained in the region of 120–350 K. Since the hydrated form exhibits a greater degree of crossover behavior in this temperature range, we shall restrict our discussion primarily to data for this compound. However, the results discussed hold equally for the nonsolvated form. Selected spectra for $[Fe(tpen)](ClO_4)_2 \cdot {}^2/_3H_2O$ are given in Figure 4. Fitting parameters for all spectra are given in Table VIII. Each spectrum was fit to two quadrupole-split doublets in a fixed area ratio of 2:1, consistent with the crystallographic results (vide supra). Only one signal is observed for each of the two unique lattice positions at all temperatures studied. Since the high-spin population of the sample is approximately 40% at 350 K, it must be concluded that

(24) (a) Cunningham, A. J.; Fergusson, J. E.; Powell, H. K. J. *J. Chem. Soc., Dalton Trans.* **1972**, 2155. (b) Sylva, R. N.; Goodwin, H. A. *Aust. J. Chem.* **1967**, *20*, 479.

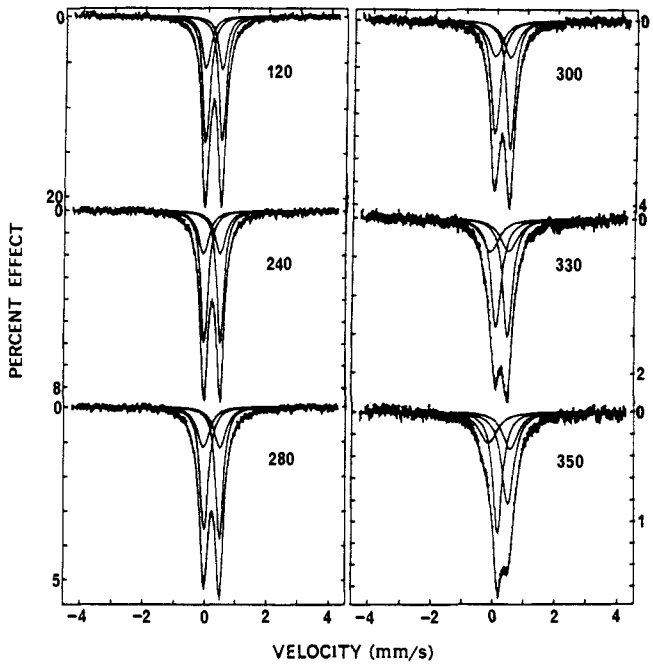

Figure 4. ^{57}Fe Mössbauer spectra of $C2/c$ symmetry [Fe(tpen)]-$(ClO_4)_2 \cdot {}^2/_3H_2O$. The inset numbers indicate temperature in degrees Kelvin.

spin-state interconversion in this complex is occurring at a rate faster than the time scale of the Mössbauer experiment implying a rate in excess of $\sim 10^7$–10^8 s^{-1}. This is the first well-documented example of a ferrous complex exhibiting an interconversion rate of this magnitude in the solid state.[25] In the case of one other complex, $Fe(phen)_2(NCBH_3)_2$, complexities seen in the Mössbauer spectrum were attributed[25a] to the presence of some Fe^{II} complexes that exhibit a fast spin-rate interconversion rate.

It must be emphasized that [Fe(tpen)]$(ClO_4)_2 \cdot {}^2/_3H_2O$ does clearly exhibit a spin-state interconversion rate that is faster than the ^{57}Fe Mössbauer time scale. The possibility that the temperature dependence of the Mössbauer spectrum illustrated in Figure 4 is due to a dehydration to the nonhydrated form can be definitively eliminated. First, as shown in a figure given in the supplementary material, the 350 K Mössbauer spectra of the hydrated and nonhydrated forms look different. Second, Mössbauer spectra for [Fe(tpen)]$(ClO_4)_2 \cdot {}^2/_3H_2O$ were first collected at 120 K and then at various temperatures up to 350 K. After this, the sample was cooled to 330 K and the spectrum was re-determined. This was followed by running spectra at several temperatures down to 150 K. These spectra were found to be the same as those obtained prior to the increase in temperature. Third, the X-ray structure of [Fe(tpen)]$(ClO_4)_2 \cdot {}^2/_3H_2O$ was determined at 358 K. Since the data collection took more than 3 days at 358 K and the unsolvated form of the complex exhibits $P2_1/c$ symmetry, it is clearly established that the H_2O solvate is not readily lost from this compound at 358 K.

The Debye temperature θ_D can be obtained from a plot of the natural logarithm of the baseline-normalized Mössbauer spectral area (A) versus temperature. For [Fe(tpen)]$(ClO_4)_2 \cdot {}^2/_3H_2O$, two straight lines can be identified in the ln (A) versus temperature plot with a change over at $\sim$240 K. Below this temperature, θ_D = 138 ± 2 K. Above 240 K, this value is reduced to 96 ± 2 K. The discontinuity in the ln (A) versus temperature plot coincides with the appearance in the magnetic susceptibility data of the high-spin species and is consistent with the smaller recoilless fraction expected for the high-spin component.

Although the most important aspect of the Mössbauer results is the implication regarding the rate of spin-state interconversion in this system, there are certain details that require some comment. Close examination of the data presented in Table VIII reveals an apparently anomalous trend in ΔE_Q with increasing temperature. As the temperature is increased, it is clear from the magnetic susceptibility studies that the percent high-spin fraction increases from approximately 10% at 300 K to 40% at 350 K. However, the change in quadrupole splitting is very modest between these temperatures. Moreover, the trend occurs in opposite directions for the two lattice sites: for site B molecules, ΔE_Q = 0.49 (4) mm s^{-1} at 300 K and increases to 0.71 (6) mm s^{-1} at 350 K; for site A molecules, ΔE_Q *decreases* from 0.49 (1) mm s^{-1} at 300 K to 0.33 (2) mm s^{-1} at 350 K.

On a qualitative basis, the observed changes in ΔE_Q can be explained by considering the sign of the electric field gradient (EFG) at each of the two sites in the lattice. Studies on other ferrous spin-crossover complexes have established that the EFG is positive for the ^{5}T state.[7a,b,26] The modest change in either direction (i.e., either at site A or site B) suggests that the sign of the EFG for the high-spin species is opposite to that of the low-spin species. Such a reversal in the sign of the EFG has ample precedent in the literature and, in fact, is the more common occurrence.[7a,b,e] This reversal in the sign of the EFG would explain the relatively small ΔE_Q for the *time-averaged* signal observed here. The opposing trends in ΔE_Q with increasing temperature can be explained by considering the lattice contribution to the EFG, EFG_{lat}. It has been shown that, particularly in the case of high-spin ferrous compounds, the lattice contribution to the total EFG can be quite substantial.[27] We suggest that EFG_{lat} is different at the two crystallographic sites. Site B, which places the molecule at a crystallographic center of inversion, will likely possess a negligible EFG_{lat} due to the fairly high symmetry of that lattice site. However, molecules at site A, sitting at a general position in $C2/c$, may experience a very different EFG_{lat}. The effect of EFG_{lat} will become more pronounced with increasing high-spin fraction, since ΔE_Q of the high-spin component is influenced more by EFG_{lat}.[7a,b,27]

This hypothesis is supported in general by changes in the asymmetry of the experimental spectra, where one component of a doublet has a line width that is larger than the other component. The reversal in the nature of the asymmetry with increasing temperature indicates that the sign of the total EFG at site A is changing with increasing high-spin fraction. In addition, the asymmetry of the two sites as determined by the experimental fit is consistent with the above argument: site B exhibits very little asymmetry, while site A undergoes significant changes with increasing temperature. A slight degree of asymmetry is evident for site B molecules in the 350 K spectrum. Note that the nature of the asymmetry is opposite to that of site A, indicating opposite signs of the EFG at the two sites. Depending on the magnitude of these differences, opposing trends in ΔE_Q with increasing high-spin fraction is a reasonable possibility.

Nature of the Spin-State Interconversion in the Solid State. Discontinuous transitions are generally associated with first-order phase transitions and occur over a range of a few degrees. By that definition alone, one would immediately describe the spin-state transition in [Fe(tpen)]$(ClO_4)_2 \cdot {}^2/_3H_2O$ as gradual from the μ_{eff} versus temperature curve (Figure 3). However, it has been shown in numerous cases that discontinuous transitions can appear gradual due to the presence of defects, impurities, and other variables.[7e,f]

For those spin-crossover systems that exhibit little or no intermolecular interaction, the spin-state transition is described by

(25) The Fe^{II} ions in the intermetallic $Fe_xTa_{1-x}S_2$ have been shown to interconvert fast on the Mössbauer time scale in the temperature region 200–500 K, see: (a) Eibschutz, M.; Lines, M. E.; DiSalvo, F. J. *Phys. Rev. B* **1977**, *15*, 103. (b) Eibschutz, M.; DiSalvo, F. J. *Phys. Rev. Lett.* **1976**, *36*, 104. (c) Lines, M. E.; Eibschutz, M. *J. Phys. Chem.* **1976**, *9*, L355. In addition, anomalous behavior that may be associated with rapid spin-state interconversion of a Fe^{II} complex has been noted in the Mössbauer spectra of $Fe(phen)_2(NCBH_3)_2$. See: (d) Edwards, M. P.; Hoff, C. D.; Curnutte, B.; Eck, J. S.; Purcell, K. F. *Inorg. Chem.* **1984**, *23*, 2613. (e) Adler, P.; Spiering, H.; Gütlich, P. *Inorg. Chem.* **1987**, *26*, 3840. (f) Bill, E.; et al. in Xavier, A. *Frontiers in Bioinorganic Chemistry*; VCH Verlag: Berlin, 1986; p 507.

(26) König, E.; Ritter, G.; Goodwin, H. A. *Chem. Phys.* **1973**, *1*, 17.
(27) Nozik, A. J.; Kaplan, M. *Phys. Rev.* **1967**, *159(2)*, 273.

Table V. Selected Bond Distances and Angles for $C2/c$ Symmetry $[Fe(tpen)](ClO_4)_2 \cdot {}^2/_3H_2O$ at 298 K

			Distances, Å		
ClA–O1	1.388 (9)	ClA–O2	1.40 (1)	ClA–O3	1.40 (1)
ClA–O4	1.41 (1)	ClB–O5	1.42 (1)	ClB–O6	1.42 (1)
ClB–O7	1.43 (1)	ClB–O8	1.42 (1)	Fe1–N1	2.022 (8)
Fe1–N2	2.044 (8)	Fe1–N3	2.020 (8)	Fe1–N4	1.977 (8)
Fe1–N5	2.046 (8)	Fe1–N6	2.005 (8)	Fe2–N7	2.018 (9)
Fe2–N8	1.996 (7)	Fe2–N9	1.967 (8)	N1–C1	1.47 (1)
N2–C2	1.46 (1)	C1–C2	1.51 (2)	N1–C3	1.49 (1)
N3–C4	1.35 (1)	C3–C4	1.49 (2)	C4–C5	1.35 (2)
C5–C6	1.38 (2)	C6–C7	1.38 (2)	N3–C8	1.34 (1)
C7–C8	1.37 (2)	N1–C9	1.48 (1)	N4–C10	1.35 (1)
C9–C10	1.50 (1)	C10–C11	1.40 (2)	C11–C12	1.34 (2)
C12–C13	1.38 (2)	N4–C14	1.35 (1)	C13–C14	1.37 (2)
N5–C16	1.33 (1)	C15–C16	1.47 (2)	C16–C17	1.40 (2)
C17–C18	1.36 (2)	C18–C19	1.34 (2)	N5–C20	1.35 (1)
C19–C20	1.38 (2)	N6–C22	1.35 (1)	C21–C22	1.49 (2)
C22–C23	1.38 (2)	C23–C24	1.36 (2)	C24–C25	1.37 (2)
N6–C26	1.33 (1)	C25–C26	1.39 (1)	N7–C27	1.48 (1)
N7–C28	1.48 (1)	N8–C29	1.35 (1)	C28–C29	1.48 (1)
C29–C30	1.40 (1)	C30–C31	1.36 (2)	C31–C32	1.36 (2)
N8–C33	1.35 (1)	C32–C33	1.38 (1)	N7–C34	1.46 (1)
N9–C35	1.37 (1)	C34–C35	1.48 (2)	C35–C36	1.38 (2)
C36–C37	1.34 (2)	C37–C38	1.37 (2)	N9–C39	1.35 (1)
C38–C39	1.42 (2)				
			Angles, deg		
N1–Fe1–N2	85.7 (3)	N1–Fe1–N3	83.2 (3)	N1–Fe1–N4	82.0 (3)
N1–Fe1–N5	98.7 (3)	N1–Fe1–N6	164.4 (3)	N2–Fe1–N3	101.7 (3)
N2–Fe1–N4	164.8 (3)	N2–Fe1–N5	82.6 (3)	N2–Fe1–N6	80.9 (3)
N3–Fe1–N4	85.6 (3)	N3–Fe1–N5	175.5 (3)	N3–Fe1–N6	91.8 (3)
N4–Fe1–N5	90.5 (3)	N4–Fe1–N6	112.4 (3)	N5–Fe1–N6	87.4 (3)
N7–Fe2–N7′	87.5 (3)	N7–Fe2–N8	83.3 (3)	N7–Fe2–N8′	96.4 (3)
N7–Fe2–N9	81.1 (3)	N7–Fe–N9′	166.7 (3)	N8–Fe2–N8′	179.6 (3)
N8–Fe2–N9	89.0 (3)	N8–Fe2–N9′	91.2 (3)	N9–Fe–N9′	110.9 (3)
O1–ClA–O2	109.4 (6)	O1–ClA–O3	110.0 (6)	O1–ClA–O4	109.2 (6)
O2–ClA–O3	110.5 (6)	O2–ClA–O4	109.7 (6)	O3–ClA–O4	108.0 (6)
O5–ClB–O6	109.5 (8)	O5–ClB–O7	109.4 (7)	O5–ClB–O8	109.5 (7)
O6–ClB–O7	109.5 (7)	O6–ClB–O8	109.5 (7)	O7–ClB–O8	109.4 (8)
Fe1–N1–C1	106.2 (6)	Fe1–N1–C3	110.7 (6)	Fe1–N1–C9	105.5 (6)
C1–N1–C3	109.5 (8)	C1–N1–C9	114.0 (8)	C3–N1–C9	110.8 (8)
Fe1–N2–C2	105.7 (6)	Fe1–N3–C4	115.2 (7)	Fe–N3–C8	125.3 (7)
C4–N3–C8	117.7 (9)	Fe1–N4–C10	113.0 (6)	Fe1–N4–C14	129.0 (7)
C10–N4–C14	118.0 (8)	Fe1–N5–C16	114.3 (7)	Fe1–N5–C20	126.2 (7)
C16–N5–C20	118.0 (9)	Fe1–N6–C22	113.0 (6)	Fe1–N6–C26	129.5 (7)
C22–N6–C26	117.5 (8)	Fe2–N7–C27	104.1 (6)	Fe2–N7–C28	111.1 (6)
Fe2–N7–C34	105.1 (6)	C27–N7–C28	110.1 (8)	C27–N7–C34	115.5 (8)
C28–N7–C34	110.7 (8)	Fe2–N8–C29	115.5 (6)	Fe2–N8–C33	126.7 (6)
Fe2–N9–C35	112.5 (7)	Fe2–N9–C39	128.4 (7)	C29–N8–C33	117.6 (8)
N2–C2–C1	108.2 (9)	C35–N9–C39	119.1 (9)	Fe2–N9′–C35	112.5 (7)
N3–C4–C5	123 (1)	N1–C3–C4	114.0 (9)	N1–C1–C2	107.4 (9)
C5–C6–C7	118 (1)	C3–C4–C5	122 (1)	N3–C4–C3	114.9 (9)
N1–C9–C10	108.2 (9)	C6–C7–C8	119 (1)	C4–C5–C6	120 (1)
C9–C10–C11	123 (1)	N4–C10–C9	115.4 (9)	N3–C8–C7	123 (1)
C12–C13–C14	118 (1)	C10–C11–C12	118 (1)	N4–C10–C11	122.0 (9)
N5–C16–C17	123 (1)	N4–C14–C13	122 (1)	C11–C12–C13	121 (1)
C17–C18–C19	122 (1)	C15–C16–C17	121 (1)	N5–C16–C15	116.8 (9)
N6–C22–C21	114.7 (9)	C18–C19–C20	119 (1)	C16–C17–C18	117 (1)
C22–C23–C24	119 (1)	N6–C22–C23	122 (1)	N5–C20–C19	122 (1)
N6–C26–C25	123 (1)	C23–C24–C25	120 (1)	C21–C22–C23	123 (1)
N8–C29–C28	116.2 (9)	N7–C27–C27′	108.8 (9)	C24–C25–C26	118 (1)
C29–C30–C31	118 (1)	N8–C29–C30	121.8 (9)	N7–C28–C29	113.0 (9)
N8–C33–C32	122.7 (9)	C30–C31–C32	121 (1)	C28–C29–C30	122.0 (9)
N9–C35–C36	120 (1)	N7–C34–C35	107.6 (9)	C31–C32–C33	118.1 (9)
C36–C37–C38	121 (1)	C34–C35–C36	125 (1)	N9–C35–C34	115.0 (9)
N9–C39–C38	122 (1)	C37–C38–C39	117 (1)	C35–C36–C37	121 (1)

a Boltzmann distribution of molecules in the low-spin ground state and the thermally accessible high-spin excited state reflecting the spin equilibrium.

$$^1A_1 \rightleftharpoons {}^5T_2 \qquad (1)$$

Such an equilibrium is generally found in solution.[7g,h] True spin equilibria are expected to be somewhat rare in the solid state, since appreciable intermolecular interactions are likely to result upon placing a molecule in a crystalline lattice. However, in the case of $[Fe(tpen)](ClO_4)_2 \cdot {}^2/_3H_2O$, a plot of ln K_{eq} versus T^{-1}, where K_{eq} was determined from magnetic susceptibility data and defined by the equilibrium represented in eq 1, is linear over the entire temperature region studied (Figure 5). From the slope of this line, it is possible to get an estimate of the zero-point energy difference, ΔE_0, between the low-spin ground state and the lowest lying spin–orbit split component of the excited high-spin state. The value of ΔE_0 was evaluated by assuming that any low-symmetry crystal field distortions are small compared to the spin–orbit splitting of the $^5T_2$ state. A spin–orbit interaction splits the $^5T_2$ state into three levels in O symmetry. The lowest energy level (Γ_5) is at energy 3λ, the next level ($\Gamma_3 + \Gamma_4$) is at λ, and the highest energy level ($\Gamma_1 + \Gamma_4 + \Gamma_5$) is at -2λ, where λ is the splitting

Table VI. Positional Parameters for $C2/c$ Symmetry $[Fe(tpen)](ClO_4)_2 \cdot {}^2/_3H_2O$ at 358 K[a]

	x/a	y/b	z/c
Fe1	0.16732 (5)	−0.2283 (2)	0.59446 (9)
Fe2	0.0	0.1842 (3)	0.75
N1	0.1347 (3)	−0.282 (1)	0.6414 (5)
N2	0.2045 (3)	−0.210 (1)	0.6776 (5)
N3	0.1398 (3)	−0.043 (1)	0.5846 (5)
N4	0.1268 (3)	−0.300 (1)	0.5281 (5)
N5	0.1928 (3)	−0.423 (1)	0.5976 (5)
N6	0.2058 (3)	−0.134 (1)	0.5725 (6)
N7	0.0364 (3)	0.022 (1)	0.7750 (5)
N8	0.0067 (3)	0.180 (1)	0.8382 (5)
N9	0.0437 (3)	0.296 (1)	0.7665 (5)
C1	0.1571 (4)	−0.314 (2)	0.7019 (7)
C2	0.1866 (4)	−0.206 (2)	0.7183 (7)
C3	0.1120 (4)	−0.162 (2)	0.6427 (8)
C4	0.1131 (4)	−0.042 (2)	0.6037 (6)
C5	0.0867 (4)	0.054 (2)	0.5879 (6)
C6	0.0899 (5)	0.161 (2)	0.5500 (7)
C7	0.1171 (4)	0.165 (2)	0.5316 (7)
C8	0.1420 (4)	0.064 (2)	0.5486 (7)
C9	0.1152 (4)	−0.403 (2)	0.6097 (7)
C10	0.1053 (4)	−0.383 (2)	0.5455 (7)
C11	0.0769 (4)	−0.452 (2)	0.5048 (8)
C12	0.0736 (4)	−0.433 (2)	0.4482 (8)
C13	0.0937 (5)	−0.347 (2)	0.4283 (8)
C14	0.1199 (4)	−0.279 (2)	0.4700 (7)
C15	0.2301 (4)	−0.328 (2)	0.6880 (7)
C16	0.2232 (4)	−0.429 (2)	0.6408 (7)
C17	0.2488 (4)	−0.528 (2)	0.6410 (7)
C18	0.2387 (4)	−0.627 (2)	0.5969 (7)
C19	0.2076 (4)	−0.626 (2)	0.5558 (7)
C20	0.1844 (4)	−0.521 (2)	0.5539 (7)
C21	0.2229 (4)	−0.075 (2)	0.6736 (7)
C22	0.2295 (4)	−0.073 (2)	0.6182 (7)
C23	0.2594 (5)	−0.016 (2)	0.6129 (8)
C24	0.2631 (5)	−0.011 (2)	0.5594 (9)
C25	0.2389 (5)	−0.071 (2)	0.5134 (9)
C26	0.2110 (4)	−0.136 (2)	0.5212 (8)
C27	0.0167 (3)	−0.106 (2)	0.7477 (7)
C28	0.0495 (3)	0.009 (2)	0.8398 (6)
C29	0.0292 (4)	0.085 (2)	0.8706 (7)
C30	0.0359 (4)	0.069 (2)	0.9301 (7)
C31	0.0187 (4)	0.153 (2)	0.9560 (7)
C32	−0.0043 (4)	0.251 (2)	0.9248 (7)
C33	−0.0094 (4)	0.263 (2)	0.8664 (7)
C34	0.0636 (4)	0.068 (2)	0.7535 (7)
C35	0.0717 (4)	0.219 (2)	0.7669 (6)
C36	0.1040 (5)	0.280 (2)	0.7781 (7)
C37	0.1070 (5)	0.417 (2)	0.7884 (8)
C38	0.0807 (5)	0.499 (2)	0.7887 (8)
C39	0.0484 (4)	0.435 (2)	0.7788 (7)

[a] Estimated standard deviations for the last significant figure are given in parentheses. The perchlorate ions are disordered at three (or four) different sites. "Idealized" perchlorate ions were refined as rigid groups: three sites for the ion centered on C11, three sites for the ion centered on C12, and four sites for the ion centered on C13. Positional parameters for these three disordered ClO_4^- ions are available in the supplementary material.

constant for the $^5T_2$ state and is given in terms of the one-electron constant ζ as $\lambda = -\zeta/2S = -\zeta/4$. The value of ζ was held constant as 420 cm^{-1}. In order to accommodate the n_{HS} versus temperature

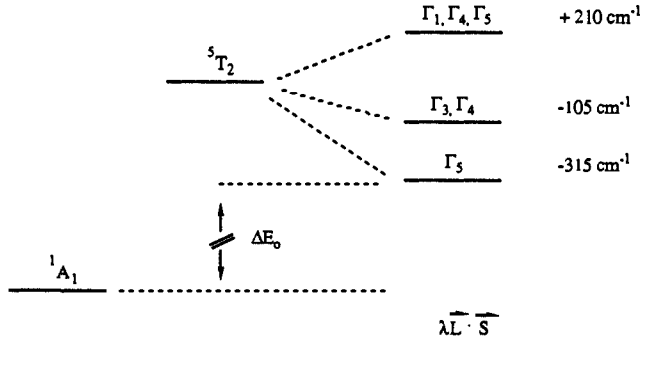

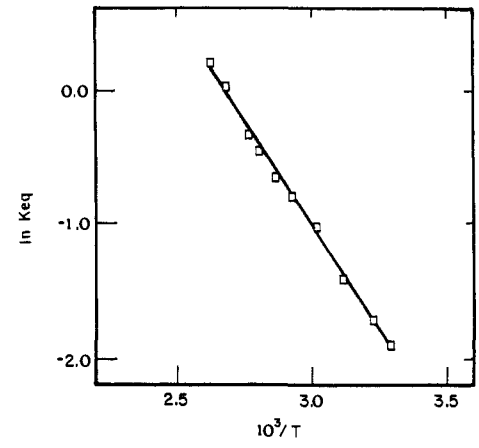

Figure 5. Plot of ln K_{eq} versus reciprocal temperature, where K_{eq} was evaluated from magnetic susceptibility for $C2/c$ symmetry $[Fe(tpen)](ClO_4)_2 \cdot {}^2/_3H_2O$.

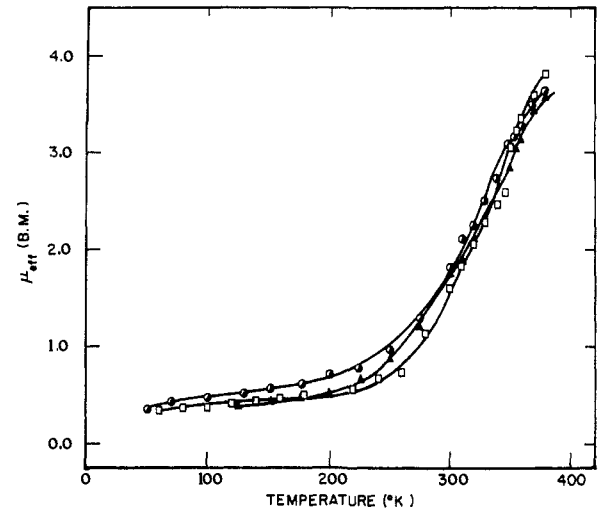

Figure 6. Plot of μ_{eff} versus temperature for $[Fe_xZn_{1-x}(tpen)](ClO_4)_2 \cdot {}^2/_3H_2O$: □, $x = 1.0$; ●, $x = 0.7$; ▲, $x = 0.5$.

data it was found that ΔE_0 (energy difference between the $^1A_1$ ground state and the triply degenerate Γ_5 level) had to vary from 617 cm^{-1} at 379.8 K and 810 cm^{-1} at 299.5 K. It is likely, therefore, that both spin–orbit interactions and low-symmetry crystal fields have to be included in the analysis. However, the present data alone probably could not be used to describe these two characteristics simultaneously.

Metal Dilution. As indicated above, although fitting of spin-crossover data to a Boltzmann model is strongly suggestive of a spin equilibrium situation, it is not conclusive. The presence of defect sites in the lattice, as well as other factors, can cause a change in the appearance of a discontinuous spin-state transition to the point where it may appear gradual, even fortuitously fit to a Boltzmann model. Likewise, the lack of any observable hysteresis in the susceptibility data does not preclude the possibility of a first-order phase transition influenced by lattice defects.[7f] Metal dilution by co-crystallization with an isostructural diamagnetic complex is an effective way to determine the existence and extent of any long-range interactions in the lattice. Power X-ray diffraction was used to determine that $[Zn(tpen)](ClO_4)_2 \cdot {}^2/_3H_2O$ is isostructural with the analogous iron compound.

The results of a dilution study are presented in Figure 6. The magnetic susceptibility of $[Fe_xZn_{1-x}(tpen)](ClO_4)_2 \cdot {}^2/_3H_2O$ for $x = 1.0$, 0.7, and 0.5 is plotted as a function of temperature. It is clear that the presence of diamagnetic $[Zn(tpen)](ClO_4)_2$ has virtually no effect on the profile of the magnetic susceptibility of the Fe^{II} compound. Similarly, ^{57}Fe Mössbauer spectra of isotopically enriched samples of the doped solid exhibit the same temperature dependence as the pure compound. Of particular

Table VII. Selected Bond Distances and Angles for $C2/c$ Symmetry $[Fe(tpen)][ClO_4)_2 \cdot {}^2/_3H_2O$ at 358 K

		Distances, Å			
Fe1–N1	2.09 (1)	Fe1–N2	2.09 (1)	Fe1–N3	2.07 (1)
Fe1–N4	2.01 (1)	Fe1–N5	2.12 (1)	Fe1–N6	2.03 (1)
Fe2–N7	2.09 (1)	Fe2–N8	2.06 (1)	Fe2–N9	2.01 (1)
N1–C1	1.48 (2)	N2–C2	1.41 (2)	C1–C2	1.54 (2)
N1–C3	1.48 (2)	N3–C4	1.32 (2)	C3–C4	1.50 (2)
C4–C5	1.37 (2)	C5–C6	1.40 (2)	C6–C7	1.33 (2)
N3–C8	1.36 (2)	C7–C8	1.37 (2)	N1–C9	1.47 (2)
N4–C10	1.35 (2)	C9–C10	1.48 (2)	C10–C11	1.41 (2)
C11–C12	1.34 (3)	C12–C13	1.36 (2)	N4–C14	1.35 (2)
C13–C14	1.37 (2)	N5–C16	1.33 (2)	C15–C16	1.45 (2)
C16–C17	1.41 (2)	C17–C18	1.38 (2)	C18–C19	1.33 (2)
N5–C20	1.37 (2)	C19–C20	1.37 (2)	N6–C22	1.34 (2)
C21–C22	1.45 (2)	C22–C23	1.39 (2)	C23–C24	1.35 (3)
C24–C25	1.35 (3)	N6–C26	1.33 (2)	C25–C26	1.37 (3)
N7–C27	1.49 (2)	N7–C28	1.48 (2)	N8–C29	1.34 (2)
C28–C29	1.48 (2)	C29–C30	1.38 (2)	C30–C31	1.35 (2)
C31–C32	1.36 (2)	N8–C33	1.36 (2)	C32–C33	1.36 (2)
N7–C34	1.45 (2)	N9–C35	1.35 (2)	C34–C35	1.49 (2)
C35–C36	1.38 (2)	C36–C37	1.33 (3)	C37–C38	1.33 (3)
N9–C39	1.36 (2)	C38–C39	1.40 (3)		
		Angles, deg			
N1–Fe1–N2	83.6 (5)	N1–Fe1–N3	81.4 (5)	N1–Fe1–N4	81.0 (5)
N1–Fe1–N5	99.3 (5)	N1–Fe1–N6	160.9 (5)	N2–Fe1–N3	103.5 (5)
N2–Fe1–N4	160.7 (5)	N2–Fe1–N5	81.2 (5)	N2–Fe1–N6	80.5 (5)
N3–Fe1–N4	85.6 (5)	N3–Fe1–N5	175.3 (5)	N3–Fe1–N6	92.0 (5)
N4–Fe1–N5	89.9 (5)	N4–Fe1–N6	116.6 (5)	N5–Fe1–N6	88.8 (5)
N7–Fe2–N7′	84.8 (5)	N7–Fe2–N8	81.2 (4)	N7–Fe2–N8′	96.9 (4)
N7–Fe2–N9	80.2 (5)	N7–Fe–N9′	162.2 (5)	N8–Fe2–N8′	177.5 (5)
N8–Fe2–N9	90.2 (4)	N8–Fe2–N9′	91.1 (4)	N9–Fe–N9′	116.1 (5)
Fe1–N1–C1	106.9 (8)	Fe1–N1–C3	110.0 (9)	Fe1–N1–C9	104.3 (9)
C1–N1–C3	109 (1)	C1–N1–C9	114 (1)	C3–N1–C9	112 (1)
Fe1–N2–C2	107.2 (9)	Fe1–N3–C4	117 (1)	Fe1–N3–C8	124 (1)
C4–N3–C8	117 (1)	Fe1–N4–C10	114 (1)	Fe1–N4–C14	128 (1)
C10–N4–C14	119 (1)	Fe1–N5–C16	112.7 (9)	Fe1–N5–C20	125 (1)
C16–N5–C20	120 (1)	Fe1–N6–C22	113 (1)	Fe1–N6–C26	128 (1)
C22–N6–C26	119 (1)	Fe2–N7–C27	104.2 (8)	Fe2–N7–C28	109.7 (8)
Fe2–N7–C34	103.5 (8)	C27–N7–C28	111 (1)	C27–N7–C34	117 (1)
C28–N7–C34	111 (1)	Fe2–N8–C29	116.8 (9)	Fe2–N8–C33	126.1 (9)
Fe2–N8′–C29	116.8 (9)	Fe2–N9–C39	128 (1)	C29–N8–C33	117 (1)
Fe2–N9–C35	115 (1)	C35–N9–C39	118 (1)	N1–C1–C2	107 (1)
N2–C2–C1	110 (1)	N1–C3–C4	115 (1)	N3–C4–C3	115 (1)
N3–C4–C5	125 (1)	C3–C4–C5	120 (1)	C4–C5–C6	115 (1)
C5–C6–C7	121 (2)	C6–C7–C8	120 (2)	N3–C8–C7	121 (1)
N1–C9–C10	111 (1)	N4–C10–C9	115 (1)	N4–C10–C11	122 (1)
C9–C10–C100	123 (1)	C10–C11–C12	116 (2)	C11–C12–C13	125 (2)
C12–C13–C14	116 (2)	N4–C14–C13	123 (1)	N5–C16–C15	118 (1)
N5–C16–C17	122 (1)	C15–C16–C17	119 (1)	C16–C17–C18	115 (1)
C17–C18–C19	123 (2)	C18–C19–C20	121 (2)	N5–C20–C19	119 (1)
N6–C22–C21	117 (1)	N6–C22–C23	121 (1)	C21–C22–C23	122 (2)
C22–C23–C24	119 (2)	C23–C24–C25	119 (2)	C24–C25–C26	120 (2)
N6–C26–C25	122 (2)	N7–C27–C27′	111 (1)	N7–C28–C29	115 (1)
N8–C29–C28	115 (1)	N8–C29–C30	123 (1)	C28–C29–C30	121 (1)
C29–C30–C31	118 (1)	C30–C31–C32	121 (2)	C31–C32–C33	118 (1)
N8–C33–C32	123 (1)	N7–C34–C35	111 (1)	N9–C35–C34	113 (1)
N9–C35–C36	122 (2)	C34–C35–C36	125 (1)	V35–C36–C37	118 (2)
C36–C37–C38	123 (2)	C37–C38–C39	118 (2)	N9–C39–C38	121 (2)

[a] A complete listing of bond distances and bond angles for the various modeled ClO_4^- ions is available in the supplementary material.

importance is the fact that the rate of spin-state interconversion with respect to the Mössbauer time scale remains unchanged: a single average quadrupole-split doublet is observed for $[Fe_xZn_{1-x}(tpen)](ClO_4)_2 \cdot {}^2/_3H_2O$ at all temperatures studied up to 350 K. On the basis of these results, we conclude that intermolecular interactions in the solid state for $[Fe(tpen)](ClO_4)_2 \cdot {}^2/_3H_2O$ are minimal. This system is best described as a solid solution, and the spin-crossover as a spin equilibrium in the solid state.

Although the metal dilution studies provide unambiguous evidence that there are no long-range intermolecular interactions in this system, the local environment still plays a vital role in determining the position of the spin-state equilibrium. Specifically, it has become clear that ΔE_0, which essentially determines the characteristics of a spin equilibrium system, can be markedly influenced by the local environment. This has been observed in this system not only in the solid state but also surprisingly in solution where ion aggregation effects on ΔE_0 have been noted in a similar system.[15b]

The cation $[Fe(tpen)]^{2+}$ exhibits spin equilibrium behavior when crystallized as a ClO_4^- salt. Salts of the cation with BPh_4^-, PF_6^-, and $CF_3SO_3^-$ all exhibit magnetic susceptibility and Mössbauer spectra characteristic of low-spin Fe^{II} up to 350 K, i.e., no spin-crossover is observed. Since the presence of a larger anion would presumably favor the high-spin species due to decreased lattice pressure, it is interesting that such is not the case in this system. It has been duly noted by other workers, however, that there is no apparent simple correlation between anion size, polarizability, etc. and the stabilization of a given spin isomer for spin-crossover complexes in the solid state.[7h] Nonetheless, it is clear that ΔE_0 is significantly different for different counterions, establishing the importance of the *local* environment for the spin equilibrium characteristics in this system.

Solution Studies. Only a few examples of magnetic susceptibility

Table VIII. ^{57}Fe Mössbauer Parameters for the $C2/c$ Symmetry $[Fe(tpen)](ClO_4)_2 \cdot {}^2/_3H_2O$

T, K		δ,[a] mm/s	ΔE_Q, mm/s	$\Gamma_{1/2}(-)$[b]	$\Gamma_{1/2}(+)$[b]
350	A[c]	0.48 (1)	0.33 (2)	0.18 (1)	0.23 (2)
	B[c]	0.36 (3)	0.71 (6)	0.34 (2)	0.29 (5)
330	A	0.43 (1)	0.38 (1)	0.20 (1)	0.18 (1)
	B	0.34 (2)	0.60 (5)	0.31 (3)	0.32 (5)
320	A	0.40 (1)	0.42 (2)	0.20 (1)	0.17 (1)
	B	0.35 (2)	0.52 (5)	0.31 (3)	0.30 (4)
300	A	0.37 (1)	0.49 (1)	0.18 (1)	0.15 (1)
	B	0.36 (2)	0.49 (4)	0.27 (4)	0.27 (3)
280	A	0.37 (1)	0.50 (1)	0.16 (1)	0.15 (1)
	B	0.36 (1)	0.55 (2)	0.25 (2)	0.24 (2)
260	A	0.37 (1)	0.50 (1)	0.15 (1)	0.14 (1)
	B	0.33 (1)	0.54 (2)	0.17 (1)	0.20 (2)
250	A	0.38 (1)	0.51 (1)	0.16 (1)	0.16 (1)
	B	0.31 (1)	0.53 (1)	0.15 (1)	0.15 (1)
240	A	0.37 (1)	0.53 (1)	0.14 (1)	0.14 (1)
	B	0.34 (1)	0.55 (2)	0.21 (2)	0.21 (2)
210	A	0.39 (1)	0.52 (1)	0.15 (1)	0.16 (1)
	B	0.31 (1)	0.54 (1)	0.15 (1)	0.14 (1)
150	A	0.38 (1)	0.50 (1)	0.16 (1)	0.16 (1)
	B	0.31 (1)	0.54 (2)	0.15 (1)	0.16 (1)
120	A	0.37 (1)	0.54 (1)	0.14 (1)	0.14 (1)
	B	0.35 (1)	0.55 (2)	0.18 (2)	0.17 (2)

[a] Center shift relative to iron foil at 300 K. [b] $\Gamma_{1/2}(-)$, half-width at height for the left side peak. $\Gamma_{1/2}(+)$, half-width at height for the right side peak. Both are given in units of mm/s. [c] The spectral area ratio of site A signal to site B signal was held fixed at 2:1 in the least-squares fitting.

Table IX. Thermodynamic Parameters for $[Fe(tpen)]X_2$ in Solution Under Different Conditions

X^-	solvent	$\Delta H°$, kcal/mol	$\Delta S°$, eu	T_c
ClO_4^-	DMF	6.31	17.4	363
ClO_4^-	2-MeOEtOH/H_2O (1:1)	5.70	16.0	356
I^-	2-MeOEtOH/H_2O (1:1)	7.08	17.8	398

measurements on spin equilibrium systems in solution have been reported in the literature.[28] One reason for this is the obvious condition that the molecular species should be stable enough in solution so as to discount the possibility of ligand dissociation. In the case of $[Fe(tpen)]^{2+}$ this condition is met,[7h] as the stability constant is on the order of 10^{25}. The commonly used technique for measuring solution susceptibility has been the Evans method,[7g] but we have found the Faraday method to be more accurate. Measurements were made at a concentration of 0.0623 M in both DMF and 50/50 mixtures of 2-methoxyethanol/H_2O in the region from 293 to 363 K. Data were obtained by both increasing and decreasing the temperature. There was no evidence of thermal hysteresis or decomposition during the course of the measurements. Plots of the effective magnetic moment, μ_{eff}, versus temperature are available in the supplementary material.

The thermodynamic parameters for the equilibrium described by eq 1 were evaluated by using eq 2 where χ_m is the experimental molar susceptibility at a given temperature, while χ_{HS} and χ_{LS}

$$K_{eq} = \frac{\chi_m - \chi_{LS}}{\chi_{HS} - \chi_m} \qquad (2)$$

are the molar susceptibilities of the pure high-spin and low-spin components at the same temperature. Plots of ln K_{eq} versus $1/T$ were found to be linear (available in supplementary material), and the thermodynamic parameters have been obtained by a least-squares fit of the data. The results are summarized in Table IX. It is evident that the solvent plays a significant role in determining the thermodynamics of the spin equilibrium, as does

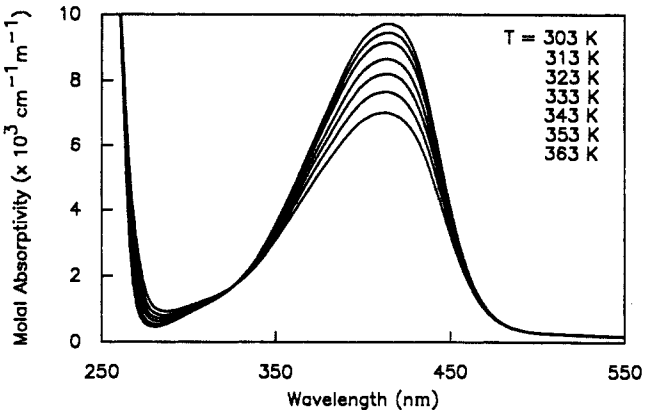

Figure 7. Electronic absorption spectrum of $[Fe(tpen)](ClO_4)_2$ in H_2O at a concentration of 1.88×10^{-4} m. Inset numbers indicate temperature in degrees Kelvin.

the identity of the counterion. In most cases it is found that the value of T_c decreases considerably on going from the solid state to solution. This is generally regarded as being due to a decrease in "lattice pressure" upon going from the solid to solution, thus stabilizing the high-spin state. In the case of $[Fe(tpen)]^{2+}$, the difference between the value of T_c in solution and the solid state is very small. This is another indication that this compound exists as a "solid solution" in the crystalline state.

The most substantial difference, in fact, arises from changing the identity of the counterion. For the ClO_4^- salt in 2-methoxyethanol/H_2O, a T_c of 356 K is found. For the I^- salt in the same solvent, this value increases by 42° to an extrapolated value of 398 K. In addition, changes in the identity of the solvent shifts the equilibrium. These observations suggest that ion aggregation in solution has a pronounced influence on ΔE_0 in this system, as was noted in laser-flash photolysis experiments.[15] Since I^- is more polarizable than ClO_4^- and will tend to form stronger ion pairs, the trend seems to be that ion aggregation results in an increase in ΔE_0, stabilizing the low-spin state.

The spin equilibrium in solution can also be monitored spectrophotometrically. Figure 7 illustrates the change in the electronic spectrum in the charge-transfer region for $[Fe(tpen)](ClO_4)_2$ in H_2O. The absorbance maximum occurs at 414 nm for the pure low-spin species and is assigned as a $^1MLCT \leftarrow {}^1A_1$ transition, although it is apparent that other bands are also present. As the high-spin component grows in with increasing temperature, the absorption becomes asymmetric and less intense overall, with the greatest drop-off occurring on the low-energy side of the band. This is reasonable, considering that the $(^1T_1,{}^1T_2) \leftarrow {}^1A_1$ ligand field bands are expected to occur in this region.[17] In addition, the overall decrease in intensity is consistent with the notion that the MLCT bands for high-spin Fe^{II} are generally less intense than those for low-spin Fe^{II} complexes. An isosbestic point at 326 nm strongly supports the presence of only two species in solution, namely the high-spin and low-spin forms of the complex. Although useful from a qualitative standpoint, quantitative interpretation of these spectra is difficult due to the ambiguity of Gaussian deconvolution.

Spin-State Interconversion Rates. There are numerous examples of ferric spin-crossover complexes exhibiting spin-state interconversion rates that are fast on the Mössbauer time scale,[29] but $[Fe(tpen)](ClO_4)_2$ is the first well-documented ferrous system to have a rate faster than can be detected by the Mössbauer technique in the solid state.[23] The fast rate found for many Fe^{III} compounds

(28) (a) Martin, L. L.; Hagen, K. S.; Hauser, A.; Martin, R. L.; Sargeson, A. M. *J. Chem. Soc., Chem. Commun.* **1988**, *19*, 1313. (b) Hoselton, M. A.; Wilson, L. J.; Drago, R. S. *J. Am. Chem. Soc.* **1975**, *97*, 1722. (c) Li Chum, H.; Vanin, J. A.; Holanda, M. I. D. *Inorg. Chem.* **1982**, *21*, 1146. (d) Jesson, J. P.; Trofimenko, S.; Eaton, D. R. *J. Am. Chem. Soc.* **1967**, *89*, 3158.

(29) (a) Maeda, Y.; Tsutsumi, N.; Takashima, Y. *Inorg. Chem.* **1984**, *23*, 2440. (b) Oshio, H.; Maeda, Y.; Takashima, Y. *Inorg. Chem.* **1983**, *22*, 2684. (c) Federer, W. D.; Hendrickson, D. N. *Inorg. Chem.* **1984**, *23*, 3861. (d) Federer, W. D.; Hendrickson, D. N. *Inorg. Chem.* **1984**, *23*, 3870. (e) Kunze, K. R.; Perry, D. L.; Wilson, L. J. *Inorg. Chem.* **1977**, *16*, 594. (f) Hall, G. R.; Hendrickson, D. N. *Inorg. Chem.* **1976**, *15*, 607. (g) Timken, M. D.; Hendrickson, D. N.; Sinn, E. *Inorg. Chem.* **1985**, *24*, 3947. (h) Maeda, Y.; Oshio, H.; Takashima, Y.; Mikuriya, M.; Hidaka, M. *Inorg. Chem.* **1986**, *25*, 2958.

is generally attributed to increased spin–orbit coupling in these compounds. For example, the high degree of covalency in the Fe–S bond for the tris(dithiocarbamate) complexes leads to increased spin–orbit interaction, and this contributes to the fast spin flipping rate found in these compounds.[29f]

In the case of a ferrous spin-crossover complex the $^1A_1$ ground state and $^5T_2$ high-spin state are involved in a spin–orbit interaction via the $^3T_1$ and/or $^3T_2$ states (assuming roughly octahedral symmetry for the sake of discussion). It is possible that, in the case of [Fe(tpen)]$(ClO_4)_2$, the $S = 1$ state(s) involved has been stabilized in energy and lies closer in energy to the low-spin and high-spin states than in other Fe^{II} complexes due to the geometric constraints of the tpen ligand. Purcell[16] has examined the effect of distortion along a trigonal twisting coordinate (a Springer-Seivers twist) on the energies of the ^1A, ^3T, and ^5T states for octahedral ferrous systems using the angular overlap model (AOM). The results of his analysis indicate that the energy of the $S = 1$ excited state is reduced as the complex is trigonally twisted. Lowering the energy of this $S = 1$ state has the same net effect as increasing spin–orbit coupling, i.e., an increased spin admixture of the low-spin and high-spin species with the intermediate state results. We have already noted that the trigonal twist angle in $[Fe(tpen)]^{2+}$ is appreciably changed relative to that expected for an octahedral system. Moreover, the average degree of distortion increases with increasing high-spin contribution, suggesting that this type of distortion may be coupled to spin-state interconversion.

We have used the structural data on [Fe(tpen)]$(ClO_4)_2 \cdot {}^2/_3H_2O$ as starting points in an AOM calculation[30] to estimate the energetic effects of a trigonal distortion on this system. The transformation simulated by these calculations is a pseudorotation where one $(py)_2N$ face of the polyhedron is rotated with respect to the other $(py)_2N$ face (i.e., the N1–N3–N4 and N2–N5–N6 planes defined above). The transformation can be described in terms of the trigonal twist angle, the angle between the two trigonal faces. The C_2 axis through the midpoint of the aliphatic backbone is preserved during the pseudorotation. Only for the trigonal prismatic structure is the molecular symmetry strictly C_{2v}. In the actual structure of $[Fe(tpen)]^{2+}$ the coordinating atoms are placed in ideal octahedral geometry; in the calculation, we used an e_σ parameter of 5.77 kK appropriate for the cation.[7h,17] We have chosen the e_π parameter as $-0.1e_\sigma$. Purcell's calculations suggest a crossing of the $S = 0$ and $S = 2$ states about midway along the pseudorotational coordinate. However, these calculations should be modified somewhat due to the pronounced drop in e_σ in going from low spin to high spin. We have estimated this change to be about 40%.[7h,17] We suggest that the pseudorotational and radial movements are synchronous. Furthermore, we anticipate spin-state isomerization and enantiomerization to occur along the same coordinate. However, to reach the crossover point, only a fraction of the full rotation would be required.

Our calculations indicate that the potential-energy minimum of the $^3T_1$ surface for [Fe(tpen)]$(ClO_4)_2 \cdot {}^2/_3H_2O$ lies approximately 2500 cm^{-1} above the $^1A_1/^5T_2$ crossing point along the trigonal twist coordinate. Combining this result with the analysis of the magnetic susceptibility data places the $^3T_1$ state at an intermediate nuclear configuration approximately 3000 cm^{-1} above the $^1A_1$ ground state. The inclusion of spin–orbit coupling in the AOM calculation would no doubt change these values somewhat, but from these results we can anticipate that the $^3T_1 \leftarrow {}^1A_1$ transition in [Fe(tpen)]$(ClO_4)_2 \cdot {}^2/_3H_2O$ will occur in the 6000–8000-cm^{-1} region. This is to be compared with the corresponding transition in the spin-crossover complex $Fe(phen)_2(NCS)_2$, to a band at 10400 cm^{-1}.[31] Thus, it is suggested by these calculations that the trigonal distortion induced by the tpen ligand contributes to a significant stabilization of the intermediate $^3T_1$ state. The increase in spin–orbit admixture of the ^3T state into the $^1A_1$ and $^5T_2$ states will lead to an increased rate of spin-state interconversion.

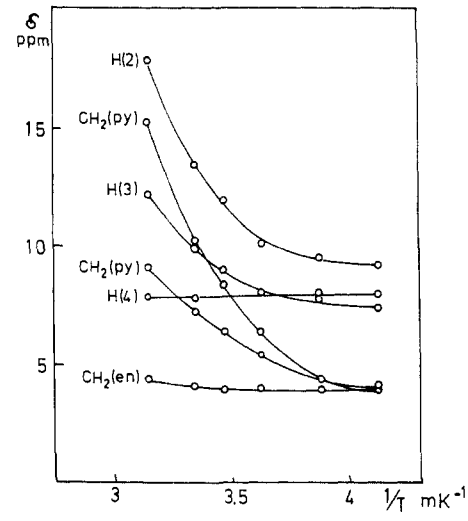

Figure 8. Plot of chemical shift versus $1/T$ for various resonances seen in the ^1H NMR spectrum of $[Fe(tpen)]I_2$ in 1:1 $MeOH/H_2O$.

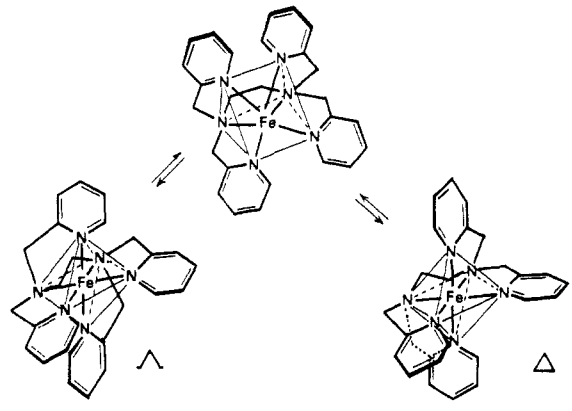

Figure 9. Schematic representation of the trigonal twist leading to molecular racemization and enantiomerization in $[Fe(tpen)]^{2+}$.

Experimental evidence suggesting fluxional behavior of $[Fe(tpen)]^{2+}$ along a trigonal twisting coordinate of this type comes from ^1H NMR studies. NMR spectra of $[Fe(tpen)]I_2$ in a 1:1 $MeOH/H_2O$ mixture in the temperature range −31 to 45 °C were recorded. (A figure showing three typical spectra is available in the supplementary material.) The results are summarized in Figure 8 where the chemical shifts of the various signals are plotted versus $1/T$. A pronounced deviation from Curie behavior due to the spin equilibrium is observed. Although the low-spin species predominates in this temperature region (see Table IX), all of the spectra are typical of labile systems. That is, the number of observed lines is about half that expected based on the known molecular structure. For example, as the pyridine groups are distributed in what formally could be described as two in axial and two in equatorial positions, a static system would be expected to give rise to two NMR signals per pyridine proton. Since only one is observed, the conclusion is that even at −31 °C the complex $Fe(tpen)^{2+}$ is fluxional. As the expected separation between the two peaks would be on the order of 150 Hz, the rate of enantiomerization at −31 °C is greater than 600 s^{-1}. The most obvious reaction coordinate for this chemical exchange is a trigonal twist, depicted in detail in Figure 9. This transformation thus also leads to molecular racemization, consistent with Purcell's analysis.[28]

To determine if a partial dissociation of the tpen ligand was occurring, experiments were performed in which $[Fe(tpen)](ClO_4)_2$ was dissolved in a dilute aqueous solution of $HClO_4$. Changes in the electronic spectrum of the sample after several *minutes* suggested the onset of initial dissociation and protonation of one of the pyridine arms of tpen. A steady-state condition was achieved after several hours, consisting of a mixture of the intact six-coordinate complex and a five-coordinate species with one pyridine

(30) (a) Schäffer, C. E.; Jorgensen, C. K. *Mol. Phys.* **1965**, *9*, 401. (b) Schäffer, C. E. *Theor. Chim. Acta* **1966**, *4*, 166. (c) Schäffer, C. E. *Struct. Bond.* **1968**, *5*, 68. (d) Schäffer, C. E. *Pure Appl. Chem.* **1970**, *24*, 361.
(31) König, E.; Madeja, K. *Inorg. Chem.* **1967**, *6*, 48.

arm protonated. The relatively long time scale for the onset of dissociation of one arm of the tpen ligand in acidic media as compared to the NMR experiment rules out the possibility of a dissociative enantiomerization process.

Conclusions. $[Fe(tpen)](ClO_4)_2 \cdot {}^2/_3H_2O$ undergoes a spin-crossover transformation with T_c = 365 K in the solid state and T_c = 363 K in a DMF solution. This is the first Fe^{II} spin-crossover complex to have a spin-state interconversion rate in the solid state which is faster than can be sensed by ^{57}Fe Mössbauer spectroscopy. The absence of intermolecular interactions, i.e., a simple spin-equilibrium for each $[Fe(tpen)]^{2+}$ complex, has been demonstrated by, inter alia, dilution studies with the isostructural Zn^{2+} complex. The results of X-ray structure determinations at 298 and 358 K show that the $[Fe(tpen)]^{2+}$ complex has an appreciable trigonal twist up and beyond what is expected for an octahedral complex. Furthermore, this trigonal twist increases as the amount of high-spin content increases. It is suggested that the trigonal twist in $[Fe(tpen)]^{2+}$ leads to an increased spin–orbit interaction between $^1A_1$ and $^5T_2$ states as a result of decreasing the energy of intermediate triplet states. This then results in an increased rate of spin-state interconversion. In solution $[Fe(tpen)]^{2+}$ exhibits a relatively fast rate of enantiomerization which supports the idea that a trigonal twisting motion is coupled to the spin-state interconversion process.

Acknowledgment. We are grateful for funding from National Institutes of Health Grant HL13652 (D.N.H.).

Supplementary Material Available: Tables of anisotropic thermal parameters for $[Fe(tpen)](ClO_4)_2$ at 298 K and $[Fe(tpen)](ClO_4)_2 \cdot {}^2/_3H_2O$ at 298 and 358 K, as well as chemical analysis, ^{57}Fe Mössbauer, and magnetic susceptibility data and figures showing Mössbauer spectra, magnetic moment vs temperature plots, and temperature dependence of the 60-MHz ^1H NMR spectrum of $[Fe(tpen)]I_2$ in 1:1 $MeOH/H_2O$ (31 pages); listing of observed and calculated structure factors (36 pages). Ordering information is given on any current masthead page.

Three Paramagnetic Reduction Stages of Phenyl-Substituted 1,2:9,10-Dibenzo[2.2]paracyclophane-1,9-dienes. Radical Anions, Triplet Dianions, and Radical Trianions As Studied by ESR and ENDOR Spectroscopy[1]

Armin de Meijere,[†,§] Fabian Gerson,*[,‡] Burkhard König,[†] Oliver Reiser,[†] and Thomas Wellauer[‡]

Contribution from the Institut für Physikalische Chemie der Universität Basel, Klingelbergstrasse 80, CH-4056 Basel, Switzerland, and Institut für Organische Chemie der Universität Hamburg, Martin-Luther-King-Platz 6, D-2000 Hamburg 13, F.R.G.
Received March 26, 1990

Abstract: Reduction of di- and tetraphenyl-substituted 1,2:9,10-dibenzo[2.2]paracyclophane-1,9-dienes, **3**, **3**-d_2, **4**, **5**, and **5**-tBu$_4$ with potassium in ethereal solvents has been monitored by ESR and ENDOR spectroscopy. In each case, the first reduction step yields a radical anion in which the unpaired electron resides in one of the two lateral biphenyl or *o*-terphenyl π-systems orthogonal to the central phane unit. Except under conditions of strong association with the K^+ counterion, electron exchange between the two π-systems is fast on the hyperfine time scale. Upon further reduction, a second electron is taken up, as revealed by the appearance of triplet dianions bearing one unpaired electron in each of the two lateral π-systems (separation ca. 1 nm). The singlet state of the dianion of **5** has been estimated to lie only slightly higher (ca. 2 kJ mol^{-1}) than the triplet state; the simultaneous presence of the singlet dianions of **3** and **5** in the solutions is compatible with evidence from NMR spectroscopy. An even more prolonged contact with potassium metal leads to radical trianions with the unpaired electron accommodated in the central phane unit. These radical trianions can thus be regarded as the radical anions of [2.2]paracyclophane having two negatively charged lateral π-systems attached to it. Detection of trianions in a quartet state by ESR spectroscopy proved to be difficult under the experimental conditions used. The sequential uptake of three electrons by **3**–**5** is discussed in the light of the reduction potentials of the constituent π-systems.

Replacement of the ethano bridging groups in [2.2]paracyclophane (**1**) by *o*-phenylenes leads to the dibenzo derivative **2**. The D_{2h} symmetry of **1** is preserved in **2**, as the planes of the lateral benzene rings are perpendicular to the mean planes of the benzene decks in the central phane unit.[2] The first synthesis of **2** was reported a few years ago.[3] More recently, not only **2** but also its derivatives **3**, **4**, and **5**, bearing phenyl substituents at the lateral rings, have become readily available via a simple preparative route.[4]

Reaction of **2** with potassium or cesium mirror in an ethereal solvent yielded a fairly persistent radical anion **2**$^{\bullet-}$, which has been studied in detail by ESR, ENDOR, and TRIPLE-resonance spectroscopy.[5] The unpaired electron in **2**$^{\bullet-}$ is accommodated

* To whom correspondence should be addressed.
† Universität Hamburg.
‡ Universität Basel.
§ Present address: Institut für Organische Chemie der Universität Göttingen, Tammannstrasse 2, D-3400 Göttingen, F.R.G.

(1) Presented, in part, at the 5th International Symposium on Organic Free Radicals, Zürich, Switzerland, September 1988.
(2) Wong, H. N. C.; Chan, C. W.; Mak, T. C. W. *Acta Crystallogr.* **1986**, *C42*, 703.
(3) Chan, C. W.; Wong, H. N. C. *J. Am. Chem. Soc.* **1985**, *107*, 4790.
(4) (a) Stöbbe, M.; Reiser, O.; Näder, R.; de Meijere, A. *Chem. Ber.* **1987**, *120*, 1667. (b) Reiser, O.; Reichow, S.; de Meijere, A. *Angew. Chem.* **1987**, *99*, 1285; *Angew. Chem., Int. Ed. Engl.* **1987**, *26*, 1277. (c) Reiser, O., Dissertation, Hamburg, 1989. (d) Reiser, O.; Khan, S. I.; de Meijere, A., manuscript in preparation.
(5) Gerson, F.; Martin, W. B., Jr.; Wong, H. N. C.; Chan, C. W. *Helv. Chim. Acta* **1987**, *70*, 79.

0002-7863/90/1512-6827$02.50/0